The Story of Flight: Daedalus and Icarus

Team 58 Project Technical Report for the 2017 IREC

Texas A&M University Sounding Rocketry Team *
Texas A&M University, Department of Aerospace Engineering, College Station, Texas

The Texas A&M University Sounding Rocketry Team has designed, built, and tested a 12 foot, 8.5 inch diameter, hybrid-powered rocket, christened Daedalus, to reach an altitude of 10,000 feet AGL while carrying two 1U satellites totaling a weight of 8.8 lbm. The team will be competing in the *10,000 feet AGL apogee with a student researched and designed (SRAD) hybrid or liquid rocket propulsion system* class of the Intercollegiate Rocket Engineering Competition at the 2017 Spaceport America Cup. The vehicle structure predominantly consists of a filament-wound carbon composite airframe with Aluminum 6061-T6 connecting bulkheads. An Aluminum 6061-T6 tail cone serves as a rigid mounting base for three removable, foam core, composite overwrapped fins as well as reduces nearly 30% of the vehicle's overall drag during the coast phase of the trajectory (as confirmed by CFD and wind tunnel testing). On board electronics consist of dissimilar redundant flight computers dedicated to initiating pyrotechnic events in the single chamber recovery bay for release of a 53 inch cruciform drogue and 120 in toroidal main chute, in addition to containing an onboard DAQ and control system for engine pressure measurements and oxidizer flow control. The entire electronics package, termed the "flight card," utilizes a minimal integration approach making it quickly transferable to any rocket the team as in its inventory. The payload consists of a high school designed nine degree of freedom measurement system and a team designed fire suppression experiment. The engine, a nitrous oxide / hydrol-terminated polybutadiene (HTPB) hybrid, named NP - 915 Icarus II, delivers a peak design thrust of 915 lbf and operates in an impulse letter range of N to a P. Team developed engine performance models and post processing codes allow for efficient and better analysis, characterization, and understanding of key engine operating principles and phenomena. To understand and predict the rocket's trajectory, the team has developed a 3 degree-of-freedom Monte-Carlo trajectory model that takes inputs from measured thrust data or engine performance models coupled with variations in atmospheric parameters to determine a distributed spread of altitudes and landing locations. This vehicle is the culmination of lessons learned during the team's first three year of existence and will provide a platform for growth and innovation for years to come.

Nomenclature

A_e	Cross sectional area of the nozzle at the exit
A_t	Cross sectional area of the nozzle at the throat
C_d	Drag coefficient of main parachute
g	Acceleration of gravity
k	Ratio of specific heats of combustion products
L	Length of nosecone
M	Mach Number at the exit
$\dot{m}$	Mass flow rate
m_{rocket}	Mass of the rocket after burnout

*Alan Aguilar Jaramillo, Ross B. Alexander, Silverio Canchola, Angel D. Castrellon, Roshan C. Doddanavar, Jacob Q. Doll, Augustus J. Ellis, Connor Farmer, Armando A. Gonzalez-Feuchter, Daniel Y. Guo, Tripp L. Illingworth, Dallas B. James, Christopher Jones, Luis E. Martinez, Sarah J. Michaels, Marshall I. Noble, Alexander E. Pages, Jacob S. Pasket, Andrew K. Riha, Julian M. Robles, Aaron R. Schiff, Andrew J. Smith, Katie L. Spira, Bradford W. Stricklin, Victoria Y. Wright

MW	Molecular weight of the combustion products
P_{cc}	Chamber pressure
P_e	Exit pressure
R	Specific gas constant
R_{base}	Outer radius
T_{cc}	Adiabatic flame temperature
v	Desired velocity of rocket during descent
V_{cc}	Chamber volume
v_e	Velocity at the exit
v_t	Velocity at the throat
x	Distance along L
ϵ	Expansion Ratio
θ_e	Exit angle (bell nozzle)
θ_n	Departure angle (bell nozzle)
ν_t	Specific volume at nozzle throat
ρ	Air density at 1500' AGL

I. Introduction

The Texas A&M University Sounding Rocketry Team (SRT) is a university recognized, student-run organization, and the only student or faculty group in the Texas A&M University system dedicated to designing, building, testing, and flying hybrid rocket systems. In addition to cultivating technical prowess, SRT expects members to develop their communication abilities through technical reports and design reviews. Beyond personal skill building, SRT promotes the next generation of passionate engineers by organizing STEM events and working with high school age students to develop payloads for flight on the rockets SRT operates.

A. Academic Program

SRT operates as a university recognized student organization which means that the team is able to utilize on-campus equipment and facilities as well as use a student organization financial management service. The university does not, however, provide any budget for its student organizations so SRT operates exclusively on sponsorships and donations. The team stores and builds most rocket components in a limited access facility dedicated to supporting the efforts of all college of engineering design classes and teams. Due to hour restrictions and shear volume handled by the facility, the team must careful plan and coordinate with the facility staff and technicians to ensure that deadlines are met. To support hybrid rocket engine testing, the team manages a test cell under the Department of Aerospace Engineering. Early years of the team custom designed and constructed the test cell infrastructure including all data acquisition and control hardware and software. This piece of infrastructure continues to evolve with the team as needs arise.

The team is made up of both Aerospace and Mechanical Engineering students within the Dwight Look College of Engineering. With the founding students and advisor coming from the Aerospace Engineering Department, the team hails as an aerospace engineering organization. The aerospace engineering academic program consists of a "modern curriculum balanced across the three principal disciplines of aerospace engineering: Aerodynamics and Propulsion, Dynamics and Control, and Materials and Structures." Senior design capstone projects include aircraft or rocket design, build, and fly, or spacecraft design. Technical electives such as chemical rocket propulsion, aerothermochemistry, and aeroelasticity, to name a few, provide a basis for work with rocket systems. SRT differs from the senior design course in that it offers a more refined environment for design and testing continuity across years (rather than a semester for each) as well as offers younger students the opportunity to develop their technical and communication skills early in their academic career.

B. Stakeholders

As stated earlier, the team operates on a sponsorship basis. Most sponsors make a one time donation and receive a certain level of recognition based on the value of their contribution. SRT-4 has received monetary

and material donations from the sponsors represented by their logos in Figure 1.

Figure 1. SRT-4 Sponsors

Additionally, many former members and personal friends of the team have made noteworthy contributions to the success of this project. Their names are listed below.

Evan Marcotte	James Pettit	Thomas Arrington	Justin Liggett	Mr. & Mrs. Gregory Doll

SRT works closely with members of Tripoli Houston, prefecture #002. Tripoli provides the team with insight as well as locations for test flights of the rocket system.

Finally, SRT recognizes the role of industry on the organization. SRT parallels many aspects of the aerospace industry with the goal of developing its members for future positions in the field. As the team continues to mature, companies which hire former members will benefit from the experience gained during their tenure on the team. Figure 2 reports a selection of the companies with the largest concentration of former and current SRT member contribution.

Figure 2. Employers of SRT Members

C. Team Structure

The Sounding Rocketry Team typically consists of 25 dedicated students ranging from freshman to graduate students. SRT has created an organizational structure to manage its large and diverse set of knowledge and skills and to facilitate both individual and team advancement. This structure is flexible and evolves each year to account for areas in the design and testing process identified as points for improvement.

This is the SRT-4 organizational structure:

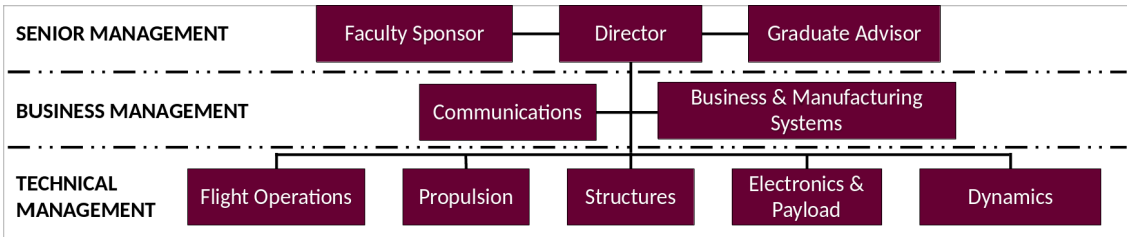

Figure 3. SRT-4 Organizational Structure

The senior management team consists of up to three people; a director, faculty sponsor, and graduate advisor. The director is student with multiple years of experience on the team, including management level experience. The directors role is to set overall short and long term objectives, increase efficiency of each sub-team, and to implement methods for increasing team transparency regarding team progress. The director also functions as the safety manager. The faculty advisor provides oversight for major projects and counsels mangers as well as members in all areas of rocket design and testing.

The business management team is a vital group responsible for the team's financial security as well as for the communication and marketing of ideas, achievements, and goals to individuals both inside and outside of the organization. SRT functions much like a start-up or research company. Coordinators selected for either of the business management sub-teams must demonstrate a strong entrepreneurial mindset and personal drive. This team works directly with the technical management core of SRT, faculty members of various departments, and influential sponsors and donors, so a high level of professionalism and maturity is required.

The technical management teams make up the core of the Sounding Rocketry Team. Each sub-team has one manager and a specified number of members to complete their dictated goals and responsibilities. The dynamics team is tasked with creating trajectory models and designing the rocket's aerodynamic surfaces (nosecone, tailcone, fins). The electronics & payload team is in charge of designing, programming, and building the rockets electronics bay and payload in addition to developing any other electrical systems needed for testing and launching. Structures role is to design, analyze, fabricate, and test all structural components of the rocket system. This includes: fabrication of new rockets and rocket components (body tubes, nosecone, fins, bulkheads, and recovery system), refurbishing of current rockets, and design and maintenance of the launch trailer and launch tower. Propulsion is expected to research, design, test, and analyze hybrid propulsion system that will be used in a flight ready engine. Flight Operations is tasked with ensuring the effective and safe launch of all systems designed by the team. This includes system refurbishment, hybrid flight-engine validation testing, system integration, recovery system design and testing, and launch day asset management.

D. Team Management Strategies

The core tenants of SRT's multi-faceted management strategy are communication, accountability, and technical competence. SRT utilizes digital, oral, and written forms of documentation and communication. Digital communication is primarily done via the Slack platform. In addition to team wide channels (chat rooms with added functionality), each sub-team manages its own channel for relevant discussion and to answer questions from other members. Each sub-team presents a weekly update presentation to the entire team about the accomplishments and setbacks of the previous week, short term goals for the upcoming week, and any additional information the sub-team may need from any of the other sub-teams. The updates are created by different members each week so sub-teams have devised various methods to ensure that all sub-team members are knowledgeable about their sub-teams progress. To further encourage intra-team understanding, presenting members are not always the same as those who created the presentation. Managers write a weekly update memo to the director the evening before the manager meeting. The director then sets meeting points and overall team goals based on the progress reported by the managers. Written documentation comes in the form of instructions sheets, media, published reports. Most of these forms of documentation are stored in the teams archive and working directory in a university-based Google drive suite. Additionally, the team has been experimenting with using OneNote, a Microsoft Office program to record and consolidate information.

To hold members and managers accountable and to aid in overall transparency, the team uses an online

program called TeamGantt to determine timelines and identify critical paths. After the director sets long term goals, each sub-team manager sets sub-team specific goals to align with the directors goals as well as work in unison with other sub-team objectives. TeamGantt consolidates all the separate timelines and provides features to determine dependencies. Additionally, the senior and technical management core uses Trello to ensure all managers are aware of their tasks and can easily see progress being made.

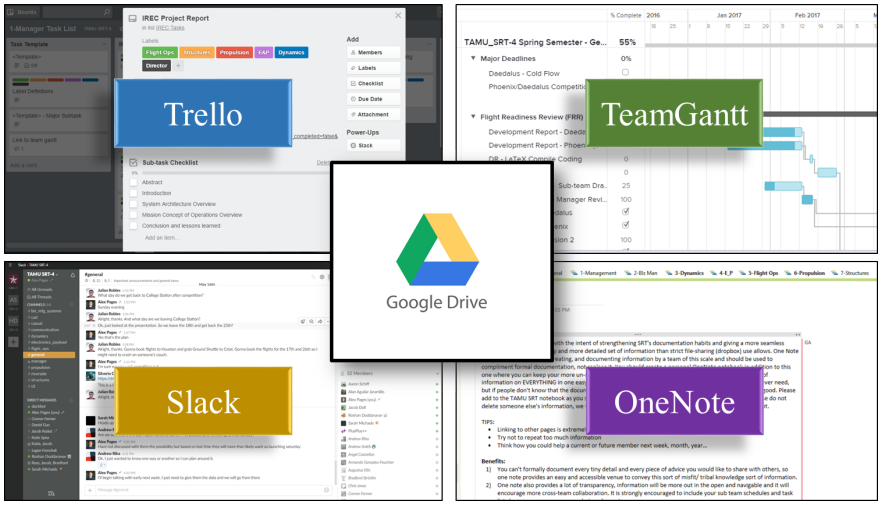

Figure 4. SRT-4 Management Strategies

II. System Architecture Overview

1. *Integrated Vehicle*

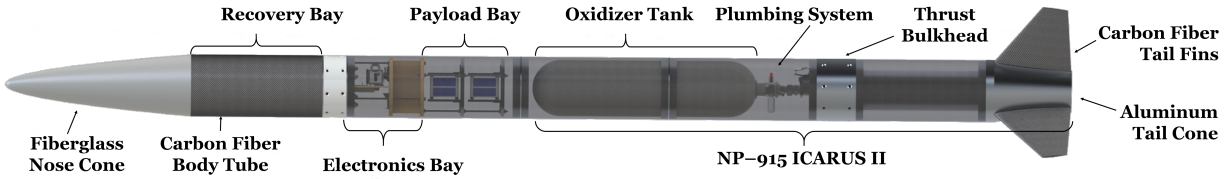

Figure 5. Daedalus - 2017 IREC/SAC Configuration

Figure 1 details the TAMU SRT-4 entry into the 2017 IREC/SAC, each specified system will be discussed in the subsequent sections.

A. Propulsion Subsystems

1. *Overview*

The Texas A&M Sounding Rocketry Team develops hybrid engines that are designed, constructed, and tested by its members. For the Daedalus vehicle, a Nitrous Oxide - HTPB hybrid engine, designated NP - 915 Icarus II, was designed to propel the rocket to 18,000 feet. It will be scaled back to launch the rocket to 10,000 feet for the 2016-2017 IREC competition.

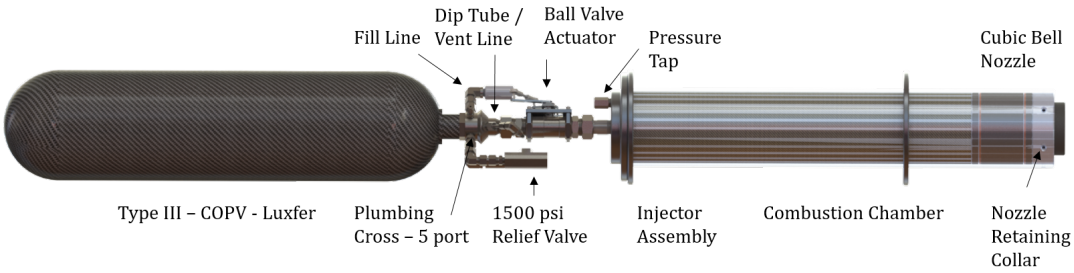

Figure 6. NP-915 Icarus II

To facilitate consistent referencing across multiple engine designs, SRT has developed a naming convention similar to that of the Tripoli Rocketry Association (TRA). Figure 7 illustrates the convention.

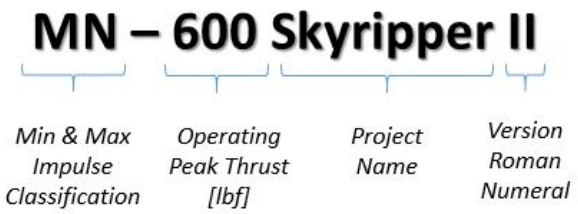

Figure 7. SRT Engine Naming Convention

For the remainder of this report, the engine will be referred to by its project name of Icarus.

2. Theoretical Model

A theoretical model of the entire engine process was developed to allow for rapid iteration through designs and to set certain propellant characteristics. The model splits the thrust curve into a liquid oxidizer flow phase and a gaseous oxidizer flow phase. The liquid phase is governed by a slightly modified algorithm developed in a thesis completed at Rochester Institute of Technology.[15] In summary, this model utilizes the ideal gas law, Rasoults Law (constant volume), and conservation of energy in the form of a forward difference to determine the phase composition, temperature (pressure from temperature derived by the Clausius-Clapeyron Equation), and mass flow rate of the oxidizer out of the tank. To model the gas phase, an modified algorithm from Aspire Space[7] iterates on a guessed value of vapor density to satisfy the ideal gas law with an estimated compressibility factor. The combustion portion of the model uses curve fitted data from algorithms based on constant pressure, constant temperature reactions minimizing Gibbs free energy (system energy). This combustion chemistry data is driven by the oxidizer to fuel ratio which is itself driven by the oxidizer mass flux through the injector. Potential energy is transferred to kinetic energy through the nozzle based on isentropic expansion principles and the frozen flow assumption. It is critical to understand that the results of this model are the theoretical maximum for the system. Real life effects such as heat transfer, combustion inefficiencies, hardware imperfections, etc. will add losses to the system not captured by this model. The team used this model in the design stages to set internal performance parameters (chamber pressure, flow rates, burn time, thrust) that translate to hardware specifications (injector area, chamber dimensions, nozzle throat, etc.).

3. Propellant - Oxidizer

Three major oxidizer options were discussed and researched for this engine; Hydrogen Peroxide, liquid Oxygen, and Nitrous Oxide. Nitrous Oxide was selected due to its relative inertness compared to other

oxidizers, ease of storage, and its ability to self-pressurize following the Clausius-Clapeyron Equation.

$$P \propto \exp \frac{\Delta H}{RT} \tag{1}$$

Figure 8 shows Nitrous Oxide pressures at given temperatures. This is assumed to be the starting oxidizer tank pressure and consequently drives the performance (peak thrust, burn time) of the entire engine.

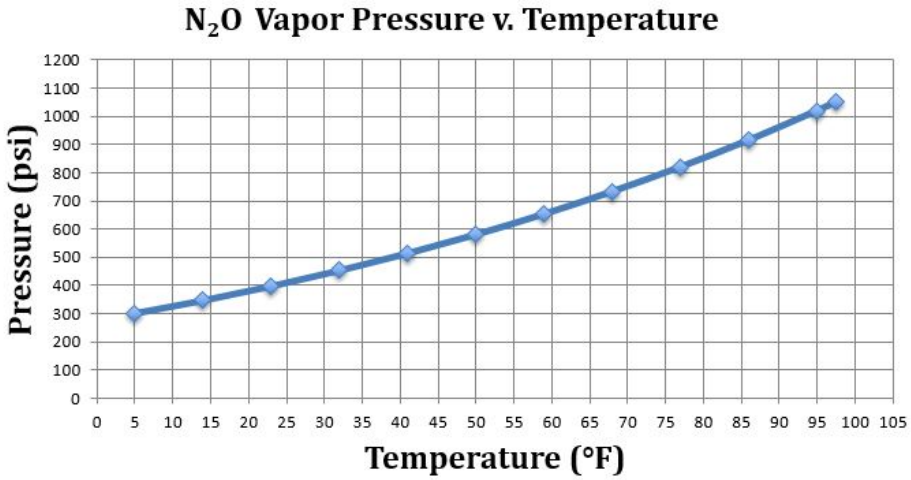

Figure 8. Nitrous Oxide Vapor Pressure

The main problem is the supercriticallity of the Nitrous Oxide; if it goes over a temperature of 97.5°F the gas phase and the liquid phases mix instead of remaining phased, violating liquid flow design assumptions at the injector and drastically reducing engine performance. Another issue with Nitrous Oxide is the susceptibility to dramatic variations in pressure and in turn, performance. To combat this variability, an insulated box with recirculating water was constructed to hold the Nitrous Oxide at a consistent desired temperature. Additionally, to facilitate filling of liquid and not gas of a standard cylinder, the fill tank is stored upside down. Figure 9 depicts the finished product complete with an in-line pressure gauge, water temperature control unit, and scale to measure fill amounts.

Figure 9. Temperature Control Box - Fill tank installed

In order to drive the filling process and ensure a full run tank, a dip tube/ vent line extends from the plumbing cross up to the top of the run tank. This feature is necessary to create a pressure differential by evacuating the air and/or oxidizer gas inside the tank and allow for an oxidizer fill. Unfortunately, the introduction of this vent line causes the liquid Nitrous Oxide to boil as it attempts to maintain its vapor pressure as mass leaves the system through the vent line. Phase changes and loss of mass through the vent

line cause a drop in temperature which reduces the pressure in accordance with Equation 1. The team has minimized these thermodynamic effects by implementing smaller vent lines and through the use of close and hold procedures which prevent mass loss and allow the system to equalize its temperature with the environment through the plumbing.

4. Propellant - Fuel

Hydroxyl-terminated polybutadiene (HTPB) was chosen as the solid fuel to be used in this engine over HDPE or paraffin wax. HDPE was eliminated due to its low regression rate and paraffin wax was removed due to its tendency to become structurally unstable (liquefy) which can potentially cause damage to the combustion chamber and nozzle. HTPB is a compromise with a relatively high chemical potential (measured using Characteristic Velocity, C* and Characteristic Specific Impulse, ISP*) and an acceptable regression rate when used with Nitrous Oxide. HTPB has plenty of literature within the rocketry community as a hybrid engine fuel facilitating in accurate modeling of its combustion with Nitrous Oxide. Equation 2 accurately represents the regression rate of hybrid fuels and the experimentally determined coefficients a and n are well documented. The design of this engine relied on the combustion modeling of this propellant. The ballistic coefficients used were a = .417 and n = .347. They were detailed in an AIAA paper from 42nd AIAA/ASME/SAE/ASEE Joint Propulsion Conference[17] and were later verified in static engine testing by comparing fuel mass lost predictions with test results.

$$\dot{r} = aG_{ox}^{n} \tag{2}$$

Using the theoretical model described earlier, the system OF ratio target was set for near stoichiometric or an OF ratio between 6.25 and 6.5. As shown in Figure 10, an output of the theoretical model, the OF ratio varies over time.

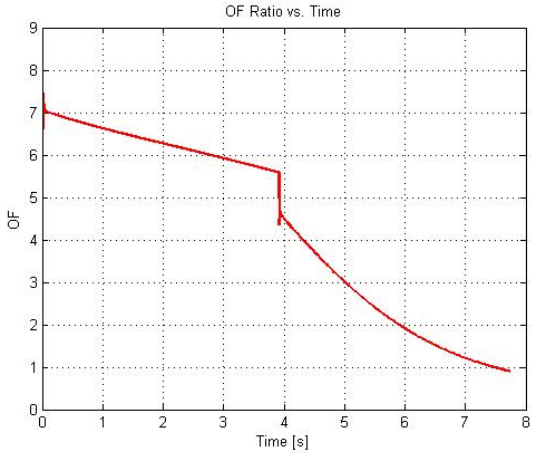

Figure 10. OF Ratio as a Function of Time

The team chose to use a circle port fuel grain for the explicit reason of more accurately comparing engine test results to the theoretical model. The HTPB fuel grain is manufactured using a two-part mixture of 83 percent HTPB-HTLO resin and 17 percent modified MDI Isocyanate curative, by weight. The mixture poured into a PVC mold with a fiberglass liner as insulation and cures for a minimum of three days before use.

5. Hardware - Tank & Plumbing

The flight oxidizer tank selected for Icarus was a Type III Composite Overwrapped Pressure Vessel (COPV) consisting of carbon composite tank with an aluminum liner. Manufactured by Luxfer Gas Cylinders, the T144A-003 has an operating pressure of 3600 psi which is more than double the maximum allowed oxidizer tank pressure (as per the relief valve setting). Additionally, this tank weighs in at 18.9 lbm, a nearly 50% reduction in some comparable aluminum tanks.

Figure 11. Plumbing System during hydrostatic test

The fill line function is self-explanatory, however to maximize the filling of the tank a vent line with a tiny orifice was incorporated to evacuate air and create the pressure differential that drives the oxidizer filling. This vent line is then kept open until the tank is full and subsequently closed off to maintain pressure. A pressure relief valve is then used to ensure that the system pressure is safely maintained below 1500 psi. Pressure transducer and thermocouple ports allow careful monitoring of the oxidizer during the filling and pre-ignition process. Quick disconnect fittings on the fill and vent lines, activated by a pneumatic piston system, safely remove the exterior lines from the vehicle before launch.

To incorporate all necessary ports, a plumbing cross was designed to reduce the number of fittings which would be needed to join them in a single line. All five of these ports connect to the major line joining the tank to the injector with a near constant area; according to mass conservation and Bernoullis principle, minimizing the changes in cross sectional area in the major line minimizes the loss in pressure. The service pressure is 5200 psi, significantly more than needed.

Oxidizer flow control was a major challenge during Icarus' development. Previous teams had attempted to actuate a ball valve using a chain and sprocket and another elaborate design involving a piston plug released by an Estes motor, both without success. Using pneumatically or electrically actuated ball valves were going to be costly, heavy, and would require a large diameter rocket to fit. Using a concept derived from a senior design class, the four-bar-linkage actuator was developed. Using a set of trigonometric equations, a spreadsheet was developed to simulate the four-bar's output torque from a given input torque. A stainless steel ball valve with the temperature, pressure, and size specifications needed was coupled with an HiTec HS-M7990TH servo motor to turn the servos 611 oz-in input into 1100 oz-in output. The ball valve, servo, four-bar linkage, and mounting hardware is collectively called the Ball Valve Actuator system (BVA).

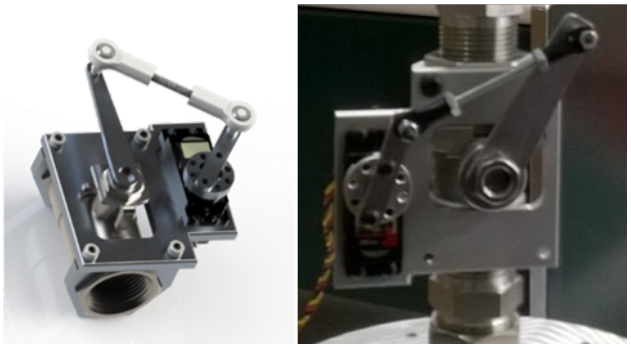

Figure 12. Ball Valve Actuator

All fittings used in the plumbing system are composed of stainless steel. Permanent connections are taped or pipe-doped NPT threads. Temporary connections meant for easy disassembly and storage of the engine or for orienting hose and sensors are tube compression or JIC fittings.

6. Hardware - Injector

The injector assembly is made up of a Aluminum 6061 T6 injector housing, a 304 Stainless Steel NPT pipe fitting machined on one end to accommodate a compression fitting, the injector coin, and top flange on the combustion chamber. Silicone and Buna-N orings provide sealing for the flange and coin respectively.

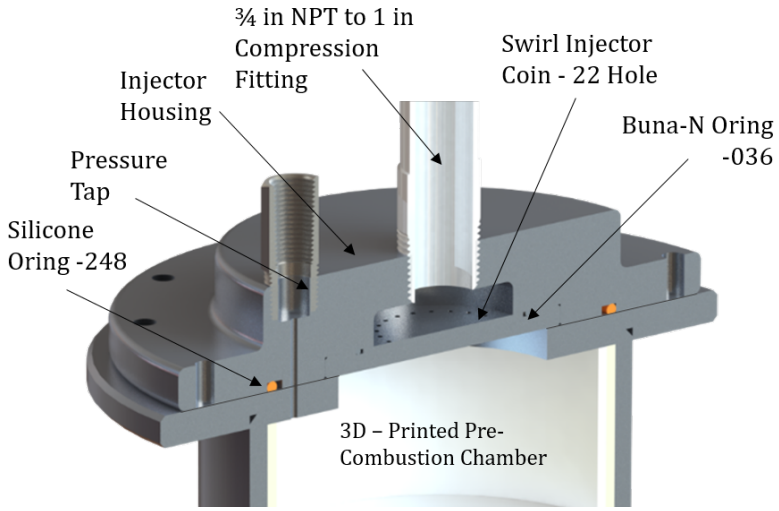

Figure 13. Injector Assembly

The injector must be able to atomize the liquid oxidizer into tiny droplets and maintain an even burn with HTPB all while maintaining a seal between the chamber and plumbing. Atomization is the process of creating small droplets in the injection, accomplished by drilling small orifices into the plate not exceeding 1.5 mm. in diameter. Small droplets are necessary because they more easily ignite and mix with the fuel better as the reaction burns. The design approach focused around finding the total injector area that provided the mass flow rate needed for an OF ratio of 6.5.

The best total area was found to be 0.0675 in^2 For atomization, this total area needs to be distributed among a number of very small orifice areas Due to machining constraints, orifice diameters of $\frac{1}{16}$ inches (0.0625 in.) were used in a total of 22 orifices.

Three specific arrangement of the orifices were considered for Icarus; axial, impinging, and swirl. The axial design holes enter straight into the chamber and into the grain port while the impinging design holes enter the chamber at an angle and converge to a central point just above the grain. Both styles were originally chosen as baseline configurations in order to gather data to compare with swirl injection and further develop the theoretical model. With swirl injection, the orifices are drilled at an angle offset from the axial direction of the rocket which effectively adds a radial component to the flow. The added radial component creates a swirl in the combustion chamber which has been shown to increase the regression rate by at least 36%[18] due to the centrifugal forces throwing the flame against the fuel grain walls. Swirl injection has been tested on similarly sized rockets with successful increased regression rates. Swirl injection was chosen as a research component for the engine design. The orifices were arranged in a circle with a 15° angle from the axial direction which maximizes the mixing of propellant along the length of the chamber. This angle also reduces the chances of blowout and to date no blowout of combustion has been observed during tests.

Figure 14. 10 May 2017 - Icaurs II Hot Fire - Fuel Grain

The top portion of the grain after the pre-combustion chamber had a localized average regression rate of about 0.254 inches per second. The rest of the fuel grain experienced an average regression rate of 0.108 inches per second. Work is being done to find ways to increase the scope of the elevated regression rate or

to harness the localized regression rate with more fuel / lower regression rate fuels.

7. Hardware - Combustion Chamber

This design is the product of several iterations of the combustion chamber from past SRT years. The basic layout of the combustion chamber was decided on the need to minimize weight, effectively transmit the engines force to the vehicle, and hold the fuel during flight. This led to a design with two flanges; the top one connected to the bottom of the vehicles thrust bulkhead, which transmits the thrust of the engine, and serves as the major connection point, and a lower one for stability during launch.

The combustion chamber houses a pre-combustion chamber for further oxidizer atomization and a post-combustion chamber built into the nozzle to allow additional stay time and a more complete combustion, all shown in Figure 7.

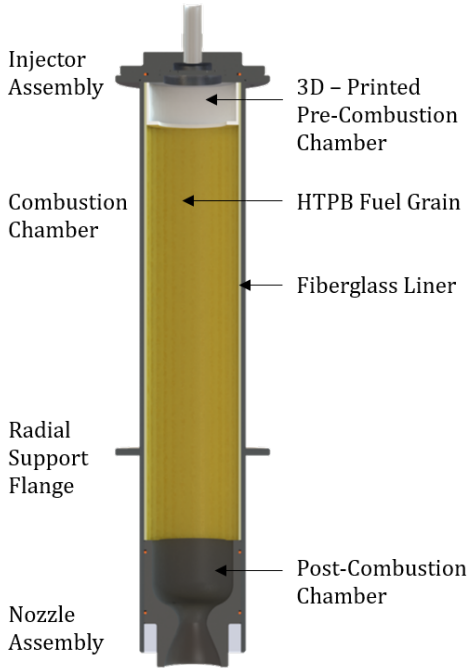

Figure 15. Icarus II - Combustion Chamber

Aluminum 6061 T6 was chosen as the material of the combustion chamber because it is light, strong, and a cost-effective material used throughout the aerospace industry. The inner diameter was sized based on the amount of fuel required to reach the design altitude of 18,000 feet (2015-16 IREC), which was done through coupled propulsion (combustion/regression analysis) and trajectory analysis. The wall thickness was initially sized to common pipe sizes and then sculpted through Finite Element Analysis (FEA) iterations to minimize weight while maintaining pressure ratings. The length was chosen based on a desired OF ratio of HTPB/NOS propellant combination modeled the EPC and taking pre-combustion and post combustion chamber needs into account.

Table 1. Combustion Chamber Specifications

Major Part	Specification	Value [in]
Tube	Length	29.85
	Outer Diameter	5.50
	Thickness	0.25
Top Flange	Outer Diameter	8.00
	Inner Diameter	3.00
	Thickness	0.38
Bottom Flange	Distance from Top Flange	18.91
	Outer Diameter	8.00
	Inner Diameter	5.50
	Thickness	0.38

A Finite Element Analysis was completed on the combustion chamber by applying a uniform expected operating pressure on the inner surfaces of the tube and top flange. As can be seen in the figure above, the current design is well below the yield stress.

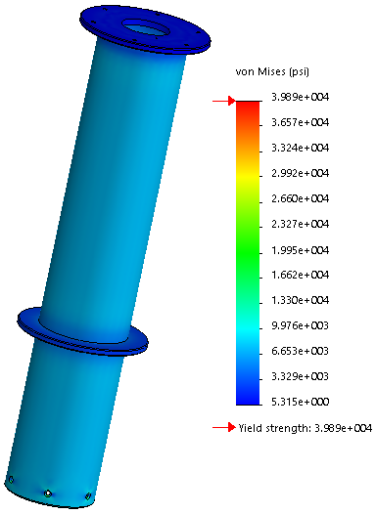

Figure 16. Combustion Chamber FEA

8. Hardware - Nozzle

The nozzle uses a converging-diverging shape to accelerate the products of combustion in the combustion chamber to high velocities before ejecting them from the rear of the rocket. As a recommendation acquired through research, the nozzle was designed to operate at the worst conditions that will occurs during flight to ensure that its performance will not fall below the required performance. All values used and presented assume isentropic flow of within the nozzle using an oxidizer to fuel ratio of approximately 6.5 and this ratio was used to determine the combustion chamber temperature Tcc, combustion chamber pressure Pcc, specific heat ratio k, and specific gas constant R.

First, the throat area was calculated by determining the velocity of the propellant exhaust at the throat, and the specific volume of the exhaust at the throat, and the average mass flow rate of propellant through the nozzle using the equations below.

$$v_t = \sqrt{\frac{2k}{k+1} RT_{CC}} \tag{3}$$

$$\nu_{CC} = \frac{RT_{CC}}{P_{CC}} \tag{4}$$

$$v_t = v_{CC}(1 + \frac{k-1}{2}M^2)^{\frac{1}{k-1}} \tag{5}$$

$$A_t = \frac{\dot{m}_p \nu_t}{v_t} \tag{6}$$

Next, the exit area must be such that the nozzle is slightly under-expanded at launch conditions, meaning that the exit pressure is slightly higher than ambient pressure conditions. This restraint ensures there are no shocks forming in the nozzle that could reduce performance and damage its structure. An exit pressure five percent higher than the ambient pressure of the competition launch site, Space Port America in New Mexico, was chosen for this design. Using this pressure, the exit area can be determined using the following equations.

$$v_{CC} = \sqrt{\frac{2k}{k-1}RT_{CC}(1 - (\frac{P_e}{P_{CC}})^{\frac{k-1}{k}})} \tag{7}$$

$$v_e = v_{CC}(\frac{P_e}{P_{CC}})^{\frac{k-1}{k}} \tag{8}$$

$$A_e = \frac{\dot{m}\nu_e}{v_e} \tag{9}$$

Finally, the contour of the nozzle was chosen with efficient expansion, weight minimization, and length minimization in mind. The best choice for this combination was the cubic bell and although it is difficult to manufacture, it outperforms both conic and parabolic nozzles. A MATLAB code with guidance from Dr. Thomas Pollock and the AERO 401 Rocket Design class was used to generate the cubic bell curve used for Icarus. This code accepts inputs for throat radius, exit radius, throat entrance and exit radii, post-combustion chamber radius, departure angle n and exit angle e, as shown in the figure. The throat entrance and exit radii inputs are taken as factors of the throat radius; factors of 1.5 and 0.4 were used, respectively, as recommended by Sutton and Biblarz in Rocket Propulsion Elements.[19] The length of the expansion section of the nozzle is determined by taking 80% of the length of a cubic nozzle with departure angle of 14 degrees for the same throat and exit radii.

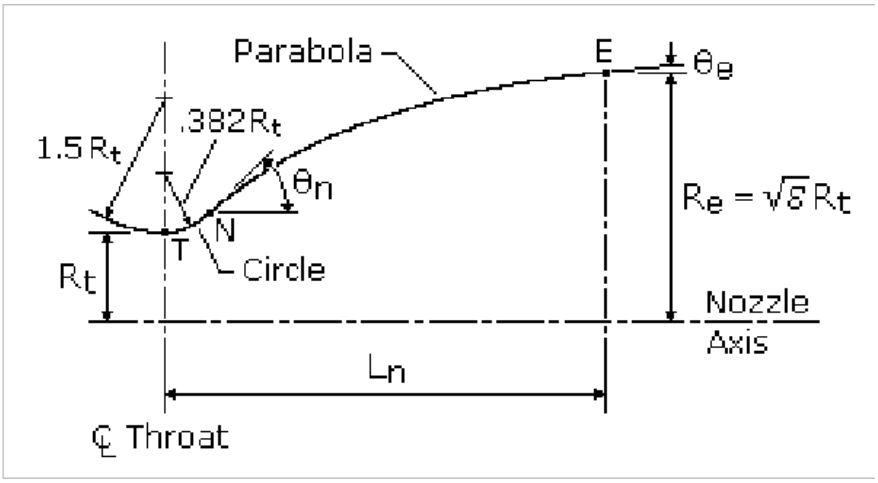

Figure 17. Definition of Nozzle Parameters

Table 2. Nozzle Specifications

Symbol	Value	Meaning
v_t	3538.9 ft/s	Velocity at the throat
k	1.253	Specific heat ratio of combustion products
R	8314.3 $\frac{J}{kmolK}$	Specific gas constant
M	2.787	Mach Number at the exit
P_{CC}	375 psig	Chamber pressure
T_{CC}	3300 K	Combustion chamber temperature
$\dot{m}$	3.07 lbm/s	Mass flow rate
MW	24.68 g/mol	Molecular weight of the combustion products
P_e	13.125 psia	Exit pressure
v_e	7473.6 ft/s	Velocity at the exit
A_t	1.628 in	Cross sectional area of the nozzle at the throat
A_e	6.859 in	Cross sectional area of the nozzle at the exit
ϵ	4.16	Expansion Ratio
θ_n	14°	Departure angle (bell nozzle)
θ_e	5°	Exit angle (bell nozzle)

The nozzle structure consists of a graphite body that contains the cubic bell contour and an aluminum collar for interfacing to the combustion chamber. Graphite was chosen largely due to its high melting point and its relatively light weight compared to other materials with similar melting points.

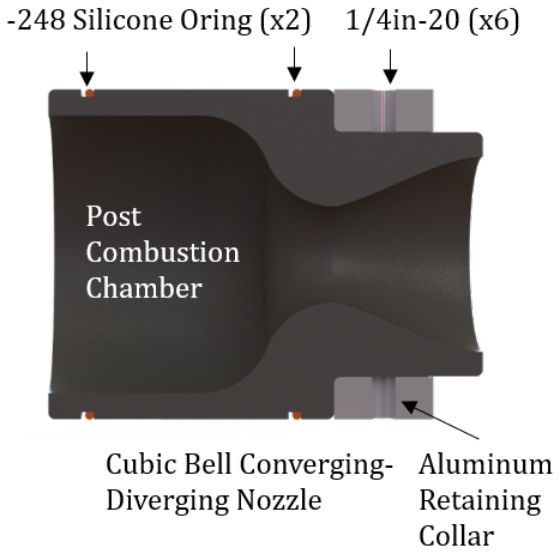

Figure 18. Nozzle/Collar Assembly

The nozzle is retained by an Aluminum 6061 T6 collar secured by six countersunk machine screws. This system was designed to be the weakest point of the combustion chamber assembly so as to be the first to fail in the event of a rapid over pressurization event. Depending on the material of bolts selected, the fail pressure can be approximately determined (heating due to burn duration introduces uncertainty). Hydrostatic testing has confirmed calculations predicting this as the primary failure mode.

B. Aerostructures

The aero structures of Daedalus were designed considering aerodynamic concerns such as speed regime effects, drag, and g-loading as well as structural variables such as strength, weight, cost, and manufacturability. Since the students on the team made a majority of the components, the manufacturability of the components and cost mainly drove the final structural design and manufacturing of the components. The aero structures of Daedalus have been flight tested and verified using a Cesaroni N25000 solid motor, producing a peak thrust of around 875 lbf and reaching an altitude of nearly 8,800 ft.

1. Nose Cone - Design

When designing the nosecone it was important to minimize drag at subsonic speeds. After researching nose cone types with various documentations two main candidates were chosen; the elliptical and the half power designs.[8910] Simulations were run in order to determine which of the two had the larger reduction in drag.

The equation for the Half-Power can be seen below with a profile of the nose cone.

$$y = R_{base}\sqrt{\frac{x}{L}} \tag{10}$$

The elliptical nose cone is created from the equation:

$$y = R_{base}\sqrt{1 - \frac{x^2}{L^2}} \tag{11}$$

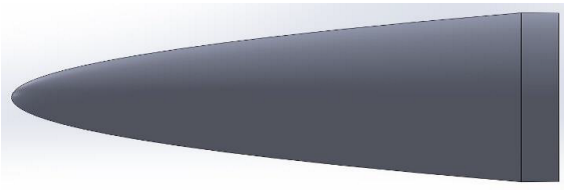

Figure 19. Half-Power Profile

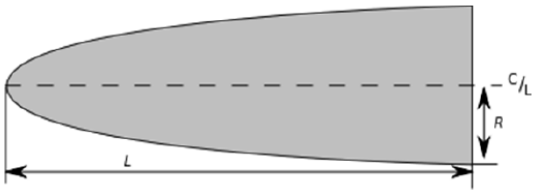

Figure 20. Elliptical Nose Cone

Computational fluid dynamics was used to determine a trend in drag and for comparison rather than determine actual Cd values. Each test was run with the same physics condition and the similar mesh continua with the simulations running at Mach 0.8. The fineness ratio of each nosecone was varied from 1 to 4 to determine the optimal ratio.

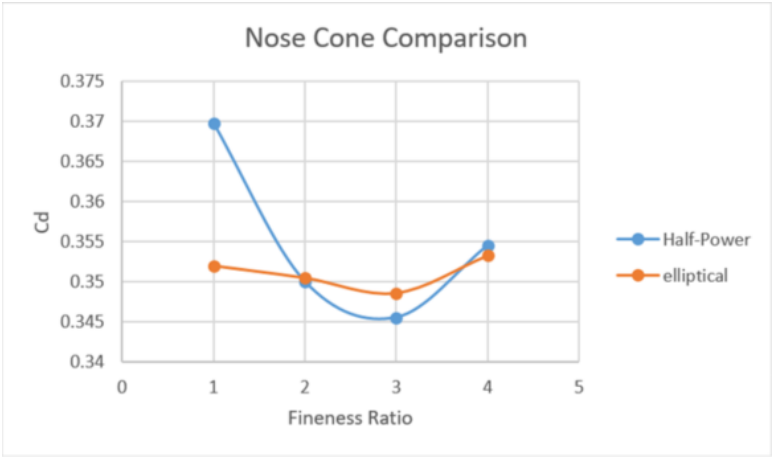

Figure 21. Comparison of Elliptical and Half-Power Data

Table 3. CFD Results

FR	Half-Power	Ellipse
1	0.369806	0.352041
2	0.350057	0.350526
3	0.34556	0.348624
4	0.354513	0.353300

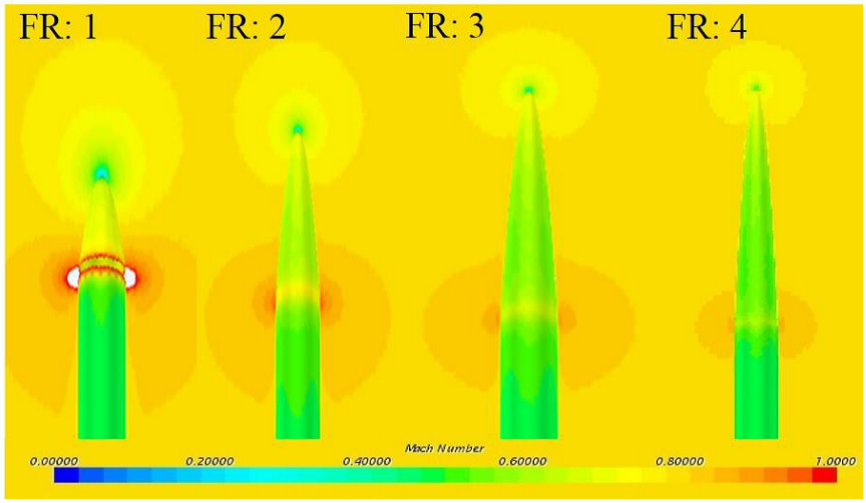

Figure 22. Half-Power Nose Cone Scene w/ Fineness Ratios

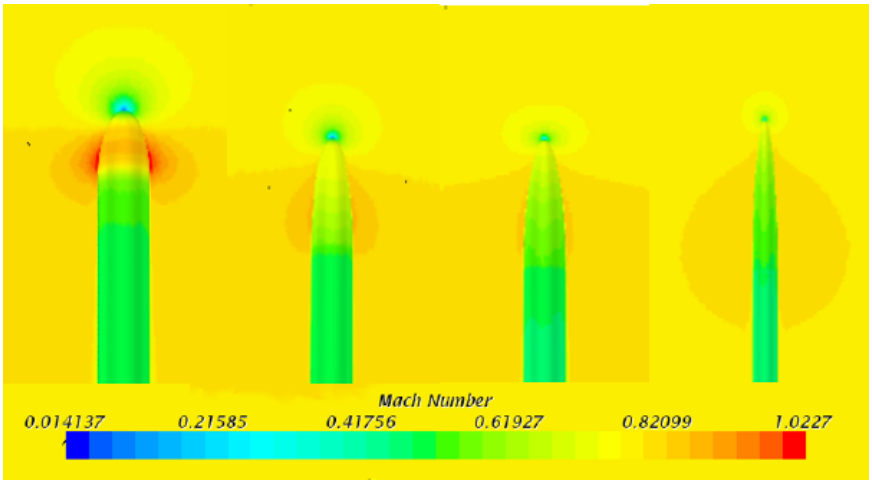

Figure 23. Elliptical Nose Cone Scene w/ Fineness Ratios

The data revealed that for both nose cone types at fineness ratio of 3:1 drag was minimized. Below a ratio of 3:1 the drag is larger due to abrupt changes in the geometry leading to larger regions of supersonic flow as can be seen in Figure 22 and Figure 23. Beyond a ratio of 3:1 skin friction drag begins to add up due to the extra length.

2. Design Conclusion

Table 4. Final Design Specifications

Half-Power	Ellipse
Fineness Ratio	3:1

From Figure 21 the data shoes us that a half-power nose cone with fineness ratio of 3:1 will minimize the drag experienced by the rocket. A key achievement was the fact that the data found from the simulations corroborated with information found in the paper, *Nose Cone Drag Study for the SStS Rocket*.[9]

3. Nose Cone - Manufacturing

The nose cone for Daedalus serves as an aerodynamic structural component, plays an integral part in the recovery system, and houses the rockets radio transmitter. The nose cone was structurally designed to withstand a compressive load of up to 1000 lbf (maximum expected peak thrust) and the tensile load of the main parachute opening with a load of 400 lbf. A key objective while designing was to maximize strength and minimize the weight of the component. Composite materials were focused on because they perform best in this area. After a material selection analysis was completed it was found that a carbon fiber-epoxy matrix offered the highest strength to weight ratio for the nose cone. However, since carbon fiber lacks radio transparency and the nose cone must house the rockets radio transmitter the material was chosen to be a fiberglass-epoxy matrix. Fiberglass was a suitable substitute which offered an acceptable strength to weight ratio and allowed radio transparency. The nose cone was manufactured using a negative mold and a hand-lay method. Figure 24 shows the nose cone after it was removed from the negative mold. This method of manufacture was selected after several failed attempts to create a nose cone using a vacuum resin transfer method, and because of its ease and final part strength. The nose cone was constructed out of three layers of fiberglass fabric due to a series of material tests which determined that one and two layers of fabric did not create suitable rigidity in the part. The material used in the construction of the nose cone was donated to the team and was the lowest cost solution. The tip of the fiberglass nose cone was removed and replaced with a 3D printed antenna assembly. This assembly allowed for easy access to the antenna, and allowed maximum radio transmission. The shoulder of the nose cone was also 3D printed and epoxied into the fiberglass body in attempt to alleviate difficulties in adding complexity to the composite works. A piece of 5-ply plywood with an U-bolt was CNC routed and epoxied into the nose cone to allow a means of recovery after it was ejected to release the parachutes.

Figure 24. Nose Cone after being removed from Negative Mold

4. Tail Cone - Design

According to a document published by the Military Technical College in Cairo, Egypt, the inclusion of a boat-tail (fins attached to transitioning geometry) or tail cone has the capability of reducing the coefficient of drag of a projectile by nearly 60 % during the coast phase of the rockets ascent.[11] It was decided that we would verify these claims and determine whether a tail cone was beneficial to the rocket. A conical design was chosen for manufacturing simplicity.

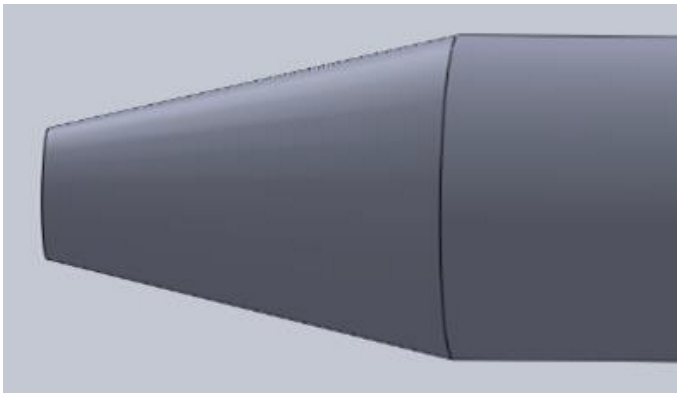

Figure 25. Tail cone

Computational fluid dynamics analysis was done to determine a trend rather than to identify actual Cd values. Two main parameters were varied, length of the tail cone and the taper angle. The results of the length simulations are shown in Figure 5.

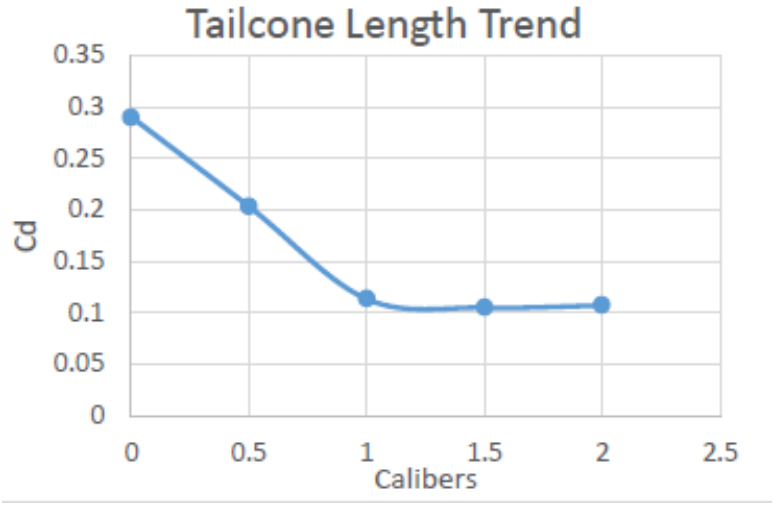

Figure 26. Tail Cone Length Trend

Table 5. Tail Cone Length Results

	Cd Reduction	Cd
No Tail	N/A	0.289770
0.5 Caliber	30%	0.202913
1.0 Caliber	61%	0.113309
1.5 Caliber	64%	0.105016
2.0 Caliber	63%	0.107139

The results of the taper angle simulations are shown in Figure 27. The taper angle trend discussed here is under the assumption that 1.25 calibers is the ideal length. Two additional tests were conducted at a taper angle of 16 degrees; one at 1 caliber in length and another at 1.5 caliber in length. This test confirmed the ideal length was indeed very close to 1.25 calibers.

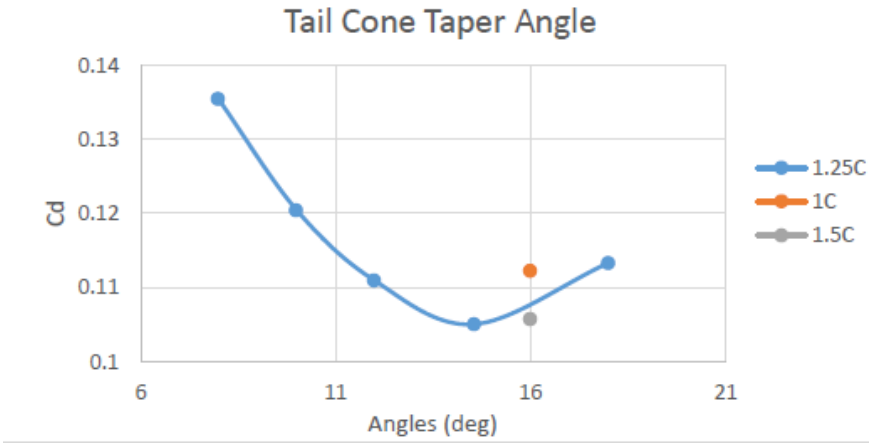

Figure 27. Tail Cone Taper Angle

From Figure 26, it can be seen that the drag reaches a minimum at around 1.25 calibers length where the combined pressure and skin friction drag are minimized. At smaller calibers pressure drag dominates as the stagnation region behind the tail cone is larger. This effect can be seen in Figure 28.

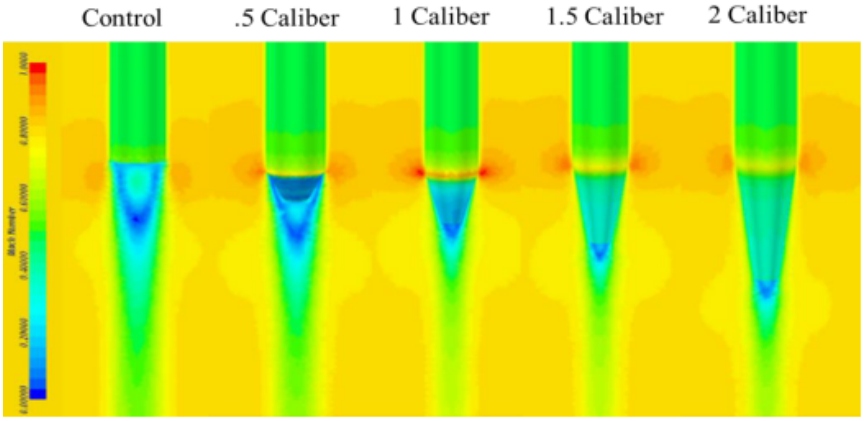

Figure 28. Direct Mach Scalar Scene Comparison

At larger calibers skin friction drag begins to become more significant and the drag begins to increase again despite the reduction in pressure drag.

With respect to the tail cone taper angle, Figure 27 shows the determined trend. Drag was shown to be minimized at a taper angle of 14.5 degrees for the same reasons as the minimum found in the length analysis. Low speed wind tunnel testing was conducted to verify the CFD simulations already done.

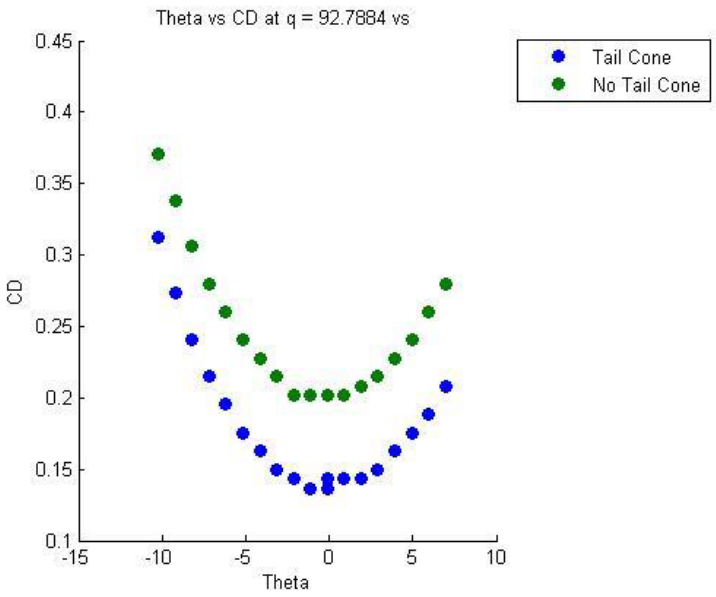

Figure 29. Tail Cone Cd Comparison

It should be noted that the tail cone tested was not at the ideal length determined by CFD simulations. Instead a length of approximately .8 calibers was used so as to fit on the wind tunnel sting assembly.

The results of the wind tunnel test with and without the tail cone are shown in Figure 29. Similar to CFD analysis, the coefficient of drag dropped with the addition of the tail cone. However, as displayed in Figure 6, the percent reduction was not as great in the wind tunnel as it was in the CFD simulations. The first and most likely cause of the discrepancy is that the sting assembly interfered with the base drag. Another possible reason for the variation in results is that the Cd reduction varies differently as the flow velocity experienced by the rocket increases.

Table 6. Tail Cone Cd Reduction Comparison

	CFD (Full Scale)	Wind Tunnel (59% Scale)
Cd	0.1468	0.1399
Cd Reduction	49.34%	30.63%

5. Tail cone - Design Conclusion

Over every medium tested (CFD and Wind Tunnel), the tail cone decreased the overall Cd significantly. With a maximum Cd reduction of 63% determined by the CFD simulations for the ideal length, the rocket would gain an additional 20.7 % in altitude. Due design alterations in response to other parameters and non-ideal conditions experienced in the real world, it is not expected that the design will perform to its maximum potential. That being said, the team believes the Cd reduction possibly is enough to warrant the incorporation of the tail cone into the final design. The ideal parameters are shown in Figure 7 and the final shape was determined by the structures team.

Table 7. Final Design Specifications

Tail cone (Y or N)	Y
Length (calibers)	1.25
Taper Angle (°)	8°-14.5°

6. Tail Cone - Manufacturing

A balance of cost, strength, and performance was crucial in the design of the tail cone for Daedalus. The tail cone was required to be stiff to prevent fin flutter, and tough to prevent failure due to impact during landing. Similar to the bulkheads, the final material of construction was selected to be aluminum 6061 due to its high strength, impact resistance, and low weight. To manufacture the tail cone a $\frac{1}{8}$ inch thick aluminum sheet was CNC plasma cut into a planar layout of a cone. The cut sheet was then rolled using a slip roller and welded at the seam. The manufacturing process significantly lowered the cost and construction time of this component when compared to other methods of production such as casting and CNC milling. During the plasma cutting phase three sets of equally spaced holes were cut to allow easy and accurate integration of the fins to the tail cone. Each fin is connected with four $\frac{1}{4}$ inch grade 8 bolts. The final manufacturing result for the tail cone was a rigid component that allowed easy integration with the fins, and improved the aerodynamics of the rocket. Figure 30 shows the fins integrated with the complete tail cone.

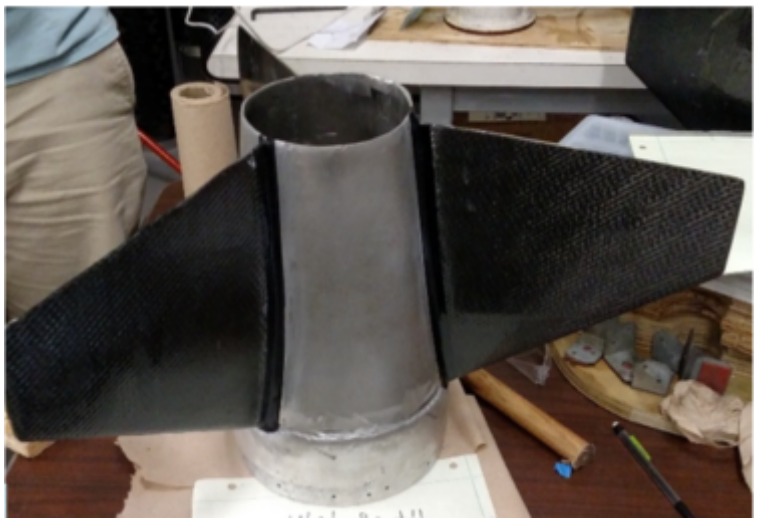

Figure 30. Final Tail Cone with Integrated Carbon Fiber - Foam Fins

7. Fins - Design

It is clear that the vehicle will spend a significant portion of its flight in the transonic regime, and as a result will be subject to aerodynamic phenomena that are characteristic of the transonic regime, such as shock-induced flow separation. After consulting with existing documentation, 3 main airfoils were selected for further analysis; the NACA 65A-010, the NASA SC(2)-0010, and the NACA/Langley Supercritical (all having a 10% thickness ratio for manufacturability. No flat-plate fins were considered since they produce a significantly lower lift force at low angles of attack and therefore provide less stability.[12]

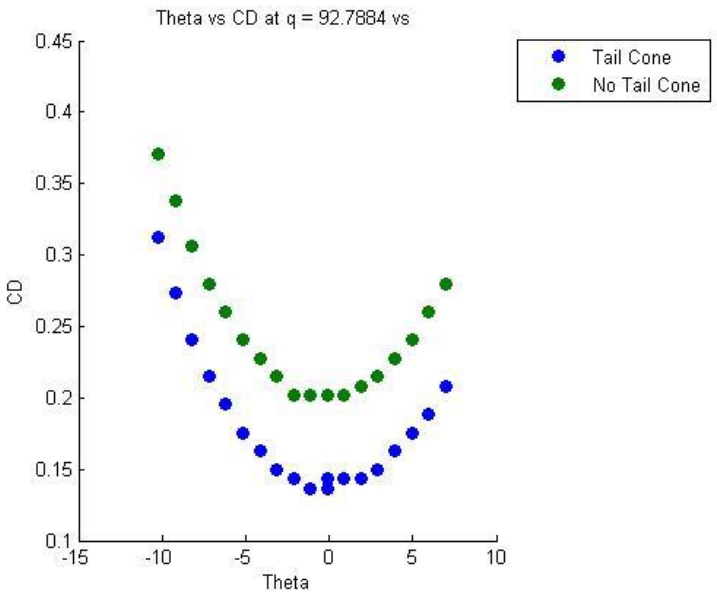

Figure 31. Airfoil Considerations

8. Surface Pressure Analysis

The three airfoils discussed previously were modeled two-dimensionally in X-foil, using an inviscid assumption and a free-stream velocity of Mach 0.8. Pressure coefficient as a function of location along the chord is presented in Figure 32

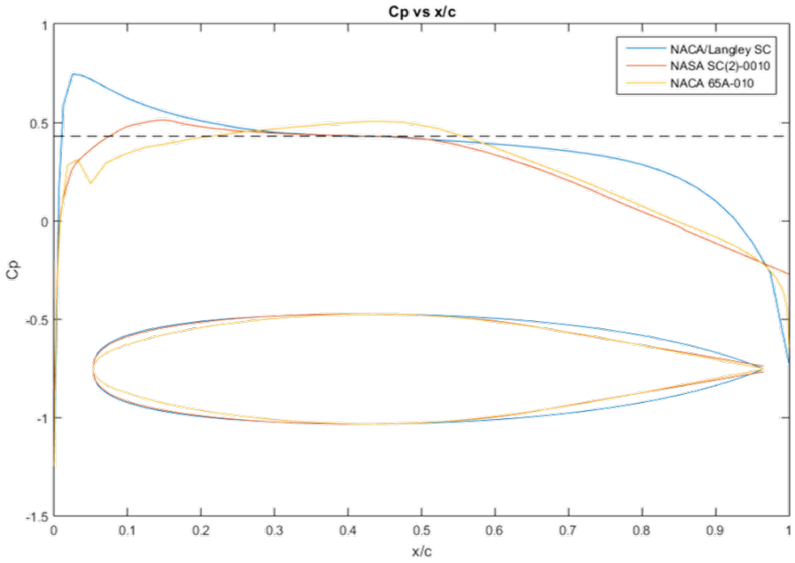

Figure 32. CP vs. X/C

The horizontal dashed line indicates the critical pressure coefficient, i.e. the point at which the local flow velocity over the surface of the airfoil becomes sonic. It can be seen that the magnitude of the pressure gradient during the second sonic transition is relatively large for the NACA 65A-010. This is an undesirable characteristic when designing for the transonic regime.[13] From this preliminary surface pressure analysis, it can be anticipated that full-scale CFD simulation will return lower drag values for the Supercritical airfoils

than for the NACA 65A-010.

9. CFD Analysis

The three airfoils were applied to a full-scale model of the vehicle, and placed in CFD simulations; the simulations were run twice, the first with a free-steam of Mach 0.8, the second Mach 0.9, both at a density altitude of 5000 ft. The results are summarized below:

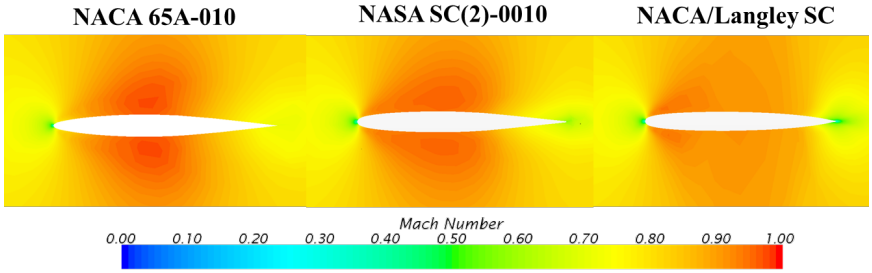

Figure 33. M = 0.8

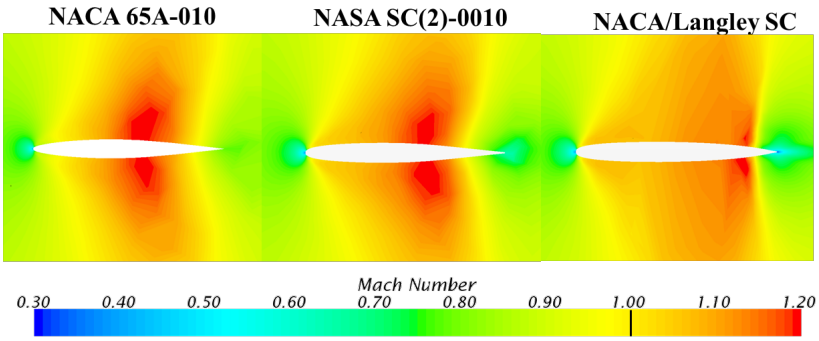

Figure 34. M = 0.9

Table 8. M = 0.8 - Tabulated Forces

	Peak Mach	Pressure (lbf)	Shear (lbf)	Total (lbf)
NACA 65A-010	0.975	25.6	30.2	55.8
NACA SC(2)-0010	0.955	25.2	30.4	55.6
NACA/Langley SC	0.943	24.7	30.4	55.1

Table 9. M = 0.9 - Tabulated Forces

	Peak Mach	Pressure (lbf)	Shear (lbf)	Total (lbf)
NACA 65A-010	1.213	64.4	36.1	100.5
NACA SC(2)-0010	1.208	58.1	36.4	94.5
NACA/Langley SC	1.218	59.1	36.3	95.4

At a free-stream of Mach 0.8, there was not enough variation between the three airfoils to come to any conclusions. However, at a free-stream of Mach 0.9, the vehicle models start to experience drag divergence, with the NACA 65A-010 causing the largest increase in drag. The reduced surface curvature discourages rapid acceleration of the flow over the mid-chord. In general, the earlier the flow expands and the less

the flow accelerates, more isentropic compression is performed by the compression waves, resulting in less non-isentropic compression that the final shock wave has to preform, leading to a weaker shock wave and decreasing the magnitude of the subsequent flow separation5.[13]

It is clear that the NACA 65A-010 is in direct conflict with transonic design principles by having a small leading edge radius that delays expansion of the flow, and substantial mid-chord curvature that encourages rapid flow acceleration.[13] From these results, it was concluded that the NACA 65A-010 was not suitable as a fin profile in this application, and that further low speed analysis would be only be conducted on the NASA SC(2)-0010 and the NACA/Langley Supercritical.

10. Low Speed Considerations

With the use of X-foil, drag polar plots were produced for both the NASA SC(2)-0010 and the NACA/Langley Supercritical. This was done at a free-stream of Mach 0.1, and with a viscous flow model that used a Reynolds number of 1e5; these conditions best imitate those which the vehicle will experience just as it has left the launch rail. The results are summarized below:

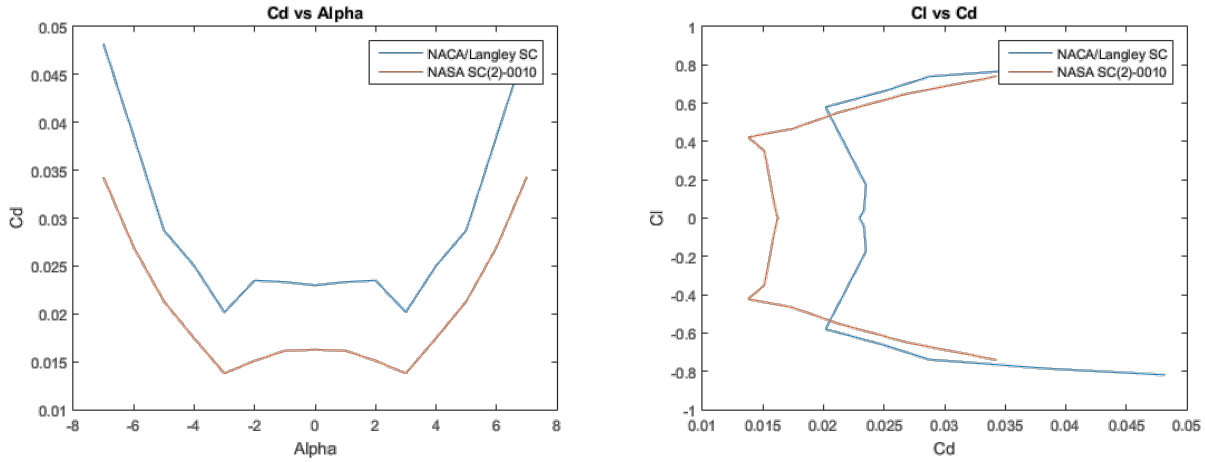

Figure 35. Super Critical Airfoils

The NASA SC(2)-0010, indicated by the orange curve, has a significantly lower drag coefficient at low angles of attack. This metric alone is enough to come to the conclusion that it has superior low-speed characteristics; for this reason, and for its favorable high-speed characteristics, the NASA SC(2)-0010 airfoil was chosen as the cross-sectional profile for the fins on this vehicle.

11. Fin Planform & Stability

To determine the optimal fin planform, center of pressure was estimated using both a set of algebraic equations produced by James Barrowman, and the amateur rocket simulation program RASAero. It was decided to use the generally accepted rule of thumb that the distance between the rockets center of pressure and center of gravity should be 1-2 calibers, or 1-2 times the maximum diameter of the rocket.[14] While determining the optimal fin planform a few restrictions were imposed. First, the root chord was held constant at the length of the tail cone. Secondly, the angle made between the plane of the base of the rocket and the trailing edge of the fins was limited to a minimum of 10 degrees in order to help protect the fins from ground impact. In order to optimize the fin planform, only one dimension was allowed to be variable at a time. Figure 36 is included to define what part of the fin is being referenced by each dimension name.

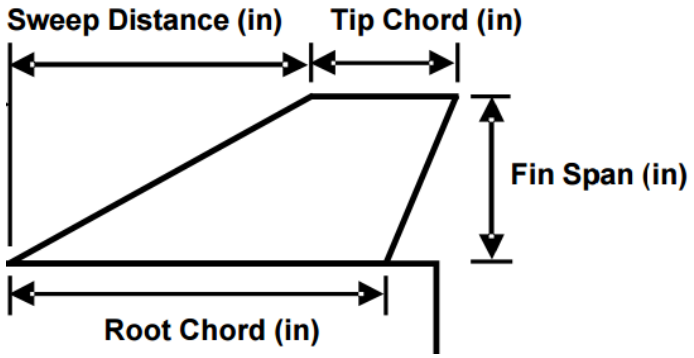

Figure 36. Fin Measurement Diagram

12. Results

There actual process of selecting the fin planform was far too lengthy to cover in this report in full detail but the results of the analysis are as follows. The lowest drag planform had a few defining characteristics. The span was as short as possible, and the sweep angle up was as low as possible (although a fin with a large forward sweep also reduced drag it was eliminated for structural reasons). When in this configuration, the tip chord had no effect on the coefficient of drag. The final dimensions are listed in Table 10, and the design is shown in Figure 37. Table 11 contains the center of pressure estimated using the original Barrowman equations, RASAero, Rogers Modified Barrowman equations, and a CFD analysis using STAR CCM.

Table 10. Final Design Specifications

Root Chord [in]	Tip Chord [in]	Sweep Distance [in]	Sweep Angle Up [deg]	Span [in]	CP [in]	Cd
10.625	2.5	6.335	10	8.5	91.876	0.213

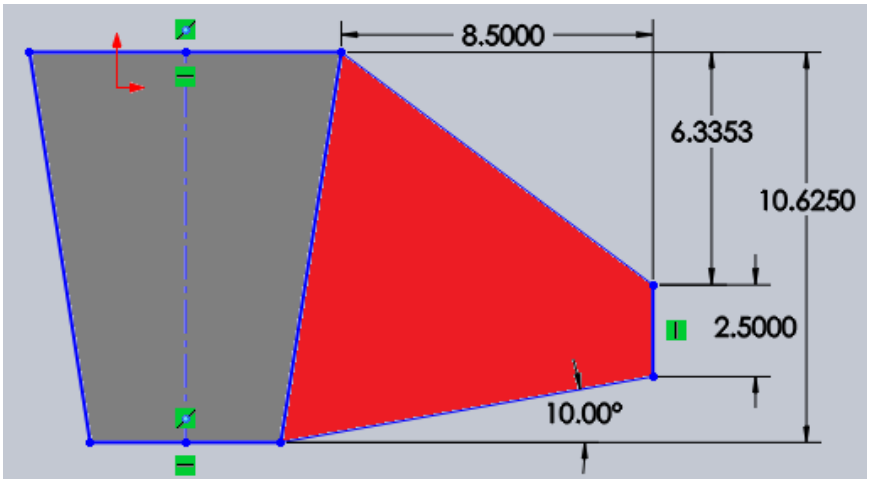

Figure 37. Final Fin CAD

Table 11. Stability Summary

Method	Center of Pressure Location [in] $\alpha = 0$	Static Stability Margin	Center of Pressure Location [in] $\alpha = 15$	Static Stability Margin
Original Barrowman Equations	83.604	0.18	N/A	—
RASAero	91.876	1.20	N/A	—
Roger Modified Barrowman Equations	97.798	1.90	90.966	1.10
CFD Analysis	109.965	3.30	104.525	2.60

13. Fins - Manufacturing

High strength and elasticity were the major design considerations for the structure of the fins. A semi-elastic fin was desired to reduce flutter at high speeds which could result in catastrophic failure of the rocket. High strength was desired to withstand the aerodynamic forces experienced during flight. A composite sandwich of carbon fiber and foam was analytically chosen by maximizing a material index of M (ratio of yield strength and density) on an Ashby chart. An aluminum base with inset steel square nuts was added to the design to facilitate attachment to the tail cone of the rocket via four $\frac{1}{4}$ inch grade 8 bolts. This design, seen in Figure 38, added modularity to the rocket and allows the team to easily replace any damaged or redesigned fins. The high-density foam core of each fin was carved by CNC router, and the aluminum base was manufactured using a CNC mill. The fin was constructed by epoxying the aluminum base to the core, and attaching the carbon fiber using vacuum-assisted resin transfer molding (VARTM) with US Composites 635 laminating epoxy. The materials used in the fins were selected because they were donated to the team, excluding the aluminum and epoxy. The end result of this manufacturing process produced fins that were very strong, lightweight and rigid, yet still retained flexibility. When flown the fins resisted fin flutter, and properly stabilized the rocket.

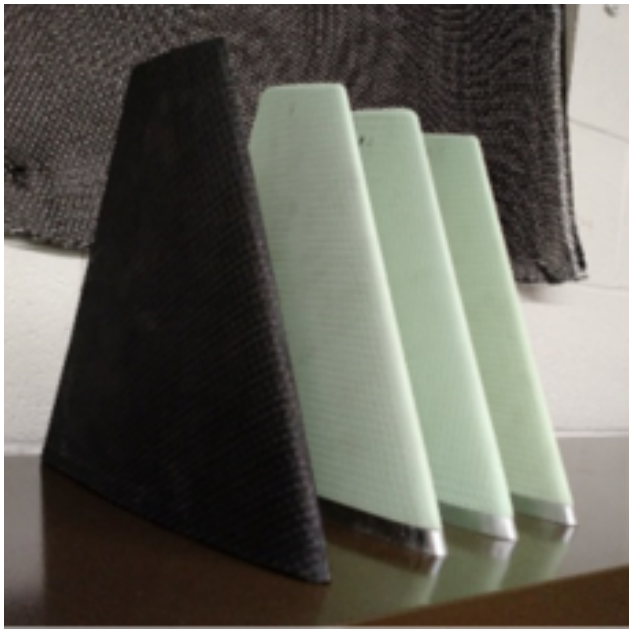

Figure 38. Modular Carbon Fiber - Foam Fin

14. Bulkheads - Design & Manufacturing

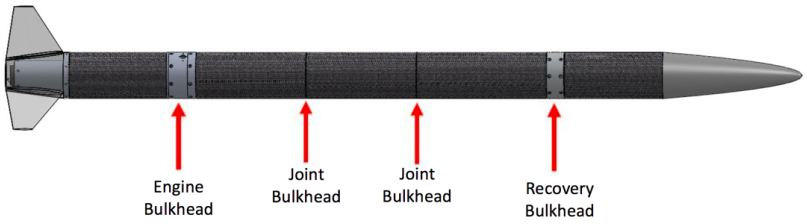

Figure 39. Bulkhead Layout of Daedalus

Daedalus bulkheads serve as a method for permanently connecting body tubes, attaching mission critical components, and transferring the thrust between rocket segments. Figure 39 shows the bulkheads that comprise Daedalus and their physical layout. Material and design constraints consisted of: weight, strength, ease of manufacturing, cost, and toughness. Of those specifications, three main material categories were considered: composites, ceramics, and metal alloys. Composites were considered for their high strength to weight ratio, but abandoned due to the difficulty of manufacturing. Ceramics were considered because of their ability to sustain large stresses and heat, but were eliminated due to their brittle nature while in tension. Aluminum alloy 6061 was chosen for the primary material for Daedalus bulkheads because of its light weight, high strength, and machinability. All bulkheads were machined by the team using manual lathes and mills.

Finite element analysis was done for bulkheads that would endure the greatest stresses. The rockets recovery bulkhead is responsible for providing a connection point between the recovery system (parachutes) and the remaining parts of the rocket. The recovery bulkhead will be under its greatest stress of 400 lbf when the main parachute of the recovery system deploys. By assuming a factor of safety of two, a stress analysis was done by applying an 800 lbf force along the U-bolts attaching the bulkhead to the recovery system (the results of this analysis can be seen in Figure 40). The results showed a maximum stress well below the yield strength of the material, and deemed the system safe for flight. Figure 40 shows the recovery bulkhead assembly that enables the team to access both the electronics bay and recovery separately, yet still allows the two sections to easily be mated together. Daedalus thrust bulkhead serves the primary function of transferring the forces due to thrust to the remaining parts of the rocket. It also serves secondary functions of providing access to engine plumbing, and to housing the engine fill lines. Similar to the recovery bulkhead assembly, the main focus of this design was to ensure a simpler assembly and ensuring the bulkhead could withstand the loads placed on it during flight. The final design was a bulkhead that could: easily connect to a flange on the combustion chamber via twelve $\frac{1}{4}$ inch vertical bolts, effortlessly mate with other parts of the rocket, allow easy access to the rockets engine, and withstand the stresses due to the thrust force. An analysis was done to ensure that the thrust bulkhead would not fail during the peak thrust of the hybrid engine of 900 lbf. The analysis was done at 1000 lbf (a conservative estimate of maximum thrust, and double the expected thrust during the competition flight) distributed along the flange where the engine would act. The results of the analysis showed a maximum stress well below the yield strength of the aluminum material. The thrust bulkhead assembly and FEA results can be seen in Figure 41.

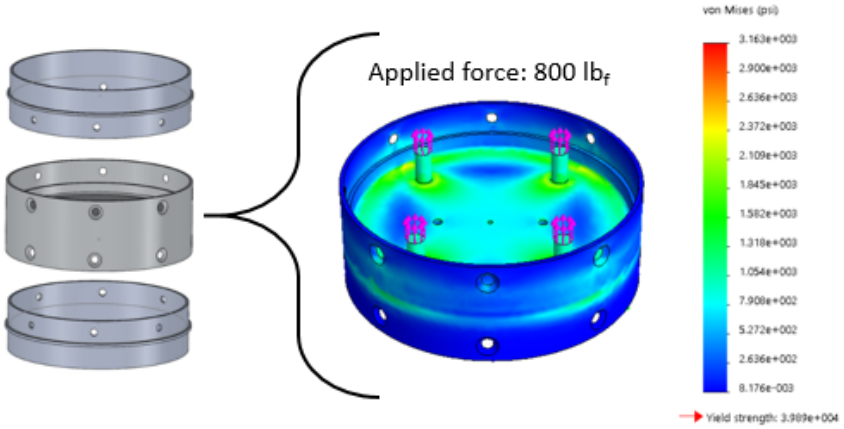

Figure 40. RecoveryBulkheadFEA

15. Body Tubes - Design & Manufacturing

The design for the body tubes of Daedalus were driven by the theoretical maximum aerodynamic forces experienced during flight. These forces were defined as the maximum compressive force during takeoff and maximum tensile force during recovery. The inner diameter of the rocket was constrained by the oxidizer tank used for propulsion. The lengths of the body tubes were constrained by the various components that

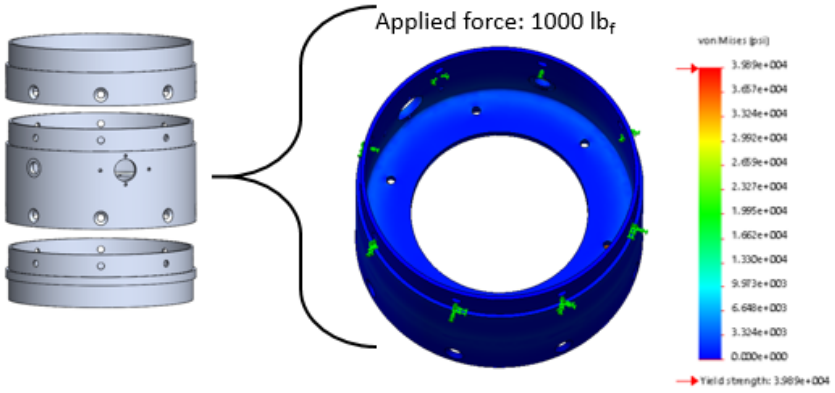

Figure 41. ThrustBulkheadFEA

they housed. For example the recovery section needed to store the parachute and recovery components and provide room to interface with the shoulder of the nose cone, and the electronics section needed to store all the necessary computers and batteries as well as the payload. A carbon fiber-epoxy composite was used in the construction of the body tubes because of its high strength to weight ratio and availability to the team. The carbon fiber used for Daedalus was donated to the team and offered the most cost effective solution to manufacturing the body tubes. Using the Toray T700S carbon fiber with a tensile fiber strength of 355 ksi, put the team well within the bounds constrained by flight conditions. Filament winding was used to manufacture the body tubes. A thick cardboard tube was used as a mandrel for winding the tow of the body tube. A 45° wind angle was used to maximize the amount of usable length of the wound body tubes. The 45° weave added shear strength to the body tubes, and still offered the strength required to handle the compressive and tensile forces of flight. The cardboard tubes were ultimately removed from the carbon fiber tubes leaving a light, stiff structure. Epoxy was chosen due to its high strength, and manufacturability. System 2000 from Fibreglast was used because it offered a tensile strength of 45.5 ksi and a compressive strength of 64 ksi, offered a long pot life, cured at room temperature, and was cost effective. Selecting this variety of epoxy for the construction of the rockets body tubes allowed the end product to withstand the forces experienced during flight, while remaining within the manufacturing budget. For sections attaching to bulkheads standard JB weld was used.

C. Recovery Subsystems

1. Parachute System

A successful recovery system meets all of the following specifications:

- Ensures safety of the launch site and surrounding areas
- Allows the rocket to be found within a reasonable distance of the launch site
- Protect the rocket from impact

A dual-deployment system consists of a smaller drogue parachute deployed at apogee and a larger main parachute which is deployed at a pre-determined altitude during the decent. This configuration allows the rocket to fall at a faster speed after apogee than it would if the main parachute were immediately deployed and minimizes the rockets displacement from the launch pad since it has less time to drift with the wind. The main parachute is deployed once the rocket is between 1500 and 1000 feet from the ground which slows the rocket for a gentle landing. If there were no drogue parachute, the rocket would fall ballistically until the main is deployed; occurring at a speed which would cause a very large inflation force that could prove harmful to the vehicle.

The recovery system consists of a recovery bay, recovery bulkhead, main parachute, drogue parachute, Advanced Retention Release Device (ARRD), 4 ejection charges (including redundant pair), kevlar y-harness, three quick links and 50 feet of tubular nylon shock cord. All of the recovery components are stored in the recovery bay and capped by the nosecone until deployment.

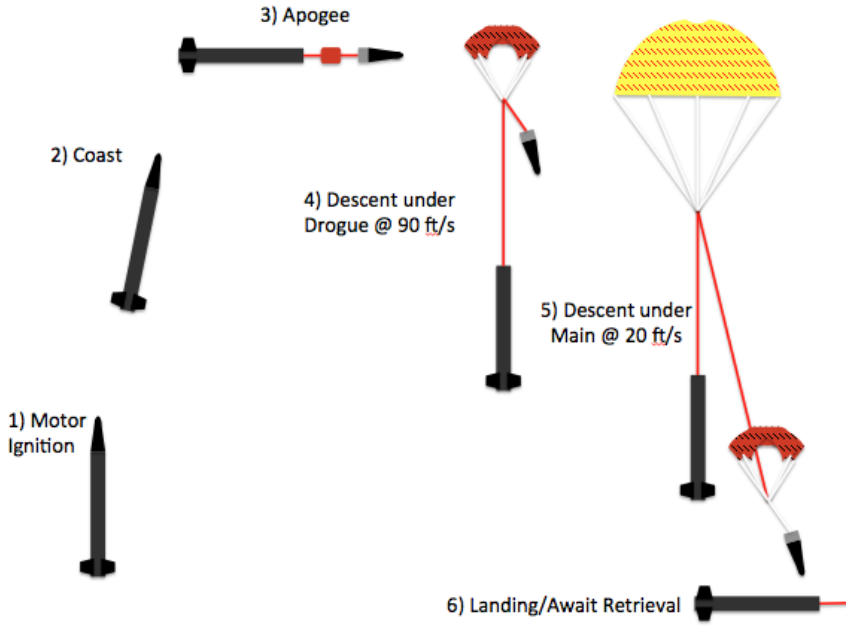

Figure 42. Recovery System Overview

The deployment of the recovery system occurs as follows:

1. The rocket reaches apogee at 10,000 feet and comes to a turning point in its vertical motion
2. The flight computer detects apogee and sets off the first ejection charge, forcing the drogue parachute to exit the airframe
3. The drogue inflates and slows the system to a velocity of approximately 90 ft/s
4. The system falls 8,500 feet for 95 seconds
5. At an altitude of 1,500 feet, the flight computer sets off the second ejection charge installed within the ARRD, releasing the main parachute
6. The main canopy fully inflates, allowing the rocket body to come to a terminal velocity of approximately 20 ft/s
7. The system falls 1,500 feet over an elapsed time of 75 seconds
8. The system impacts the ground and awaits retrieval 165 seconds after leaving the launch pad

The ARRD is used to hold the shock cord to the recovery bulkhead until the main parachute is ready for deployment. Once the vehicle is 1500 ft above ground level the pyrodex charge in the ARRD is ignited and the shackle holding the shock cord is released. The drogue acts as a pilot chute to guide the main out of the recovery bay.

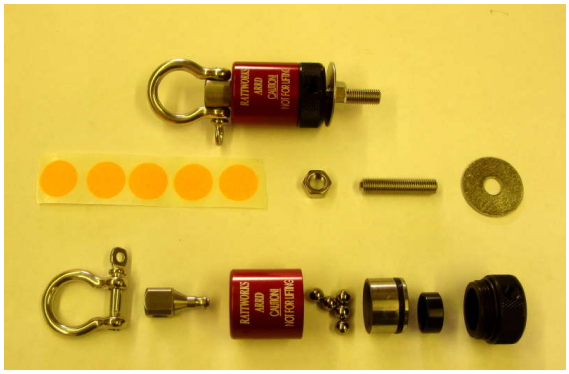

Figure 43. ARRD by Rattworks

The airframe, drogue, and main parachute are linked by the shock cord. The shock cord is 1 tubular mil-spec nylon strap. This material was chosen due to its tensile strength, durability, and fire resistivity. Since the shock cord is a load-bearing component, the material must be rated to withstand the force exerted on the rocket by the parachutes during deployment.

All components of the recovery system are subject to the opening force of the main parachute, caused by the time rate of change of momentum of the rocket. Impulse-momentum theory is used to derive an expression that relates the parachute parameters, atmospheric conditions, parachute inflation time, and velocities of the system which quantifies the magnitude of this exerted force. Using the projected weight for the propellant free system (dry rocket) and specifications

Table 12. Recovery System Max Load Ratings by Component

Component	Max Load [lbs]
Shock cord	4000[1]
Swivel	3000
3/8" Quick-link	6000
Kevlar Y-harness	6000
ARRD	2000[2]

[1] Max load reduced by a factor of 2 due to knotted connections in shock cord

[2] System has been tested to 3100 lbs before failure

of the main parachute, opening forces can shown to be a function of inflation time. The opening force is expected to be 400 lbs which gives the lowest rated component of our system a factor of safety of 5.8 using an approximate inflation time of 3-4 based on data from previous flights and tests.

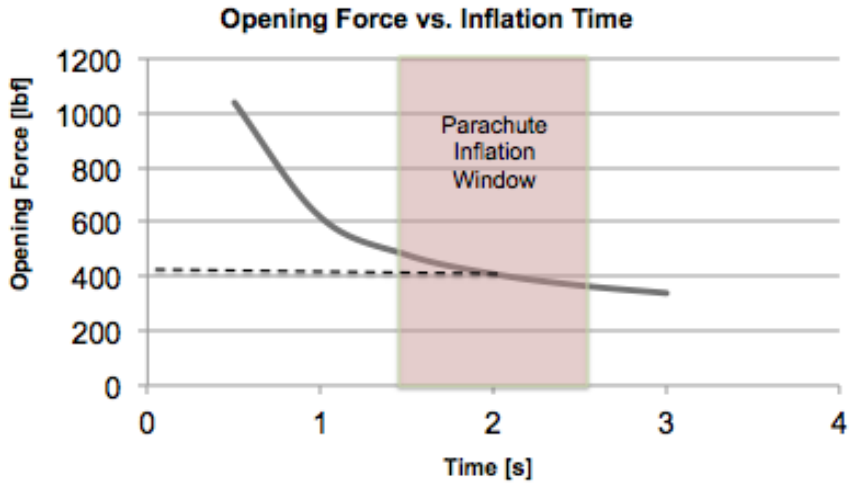

Figure 44. Opening force as a function of parachute inflation time derived from impulse-momentum theory

Drag coefficient, relative stability, simplicity of design, and ease of fabrication were all considered when evaluating canopy shapes and designs for both the main and drogue chutes.

Solid and slotted canopies are the two most commonly used parachutes. Solid canopies have a continuous area constructed from fabric gores, or panels, and might include a central vent hole. Solid canopies, therefore, are less porous and have a higher coefficient of drag making them an ideal choice for a main parachute. Slotted canopies feature multiple horizontal vents and have a higher porosity than solid canopies; making them common options for near-supersonic speed drogues. We decided on a cross shape solid canopy for our drogue after taking into account the fabrication challenges of slotted canopies and since it will experience a much slower decent velocity (90 ft/s). The industry standard for both canopy designs is zero-porosity rip-stop nylon.

A force balance between the approximate weight of the rocket under gravity and the drag created by each parachute allows us to derive an expression for the parachutes size as a function of the coefficient of drag, weight of the rocket, and desired velocity for each decent phase as shown below.

Setting the drag of the parachute equal to the weight of the rocket we find an equilibrium state equation

$$\frac{1}{2}\rho v^2 C_d S = m_{rocket} g \tag{12}$$

Substituting an expression for the 2D projection of the parachute area and rearranging for S we find

$$\text{Parachute Diameter} = \sqrt{\frac{8m_{rocket}g}{\pi\rho v^2 C_d}} \tag{13}$$

Table 13. Parachute Design Specifications

	Main Chute	Drogue Chute
Manufacturer	Fruity Chutes	SRT (in-house)
Name	Iris Ultra	Cross Parachute
Type/Shape	Annular	Cross
Dimensions	120 inches	53 inches x 53 inches
Weight	36 ounces	4 ounces
Shroud Line Max Rating	400 lbs x 12 lines	250 lbs x 8 lines

The main parachute was purchased from a high power rocketry retailer instead of fabricated in-house to ensure stronger stitched joints between gores, a more symmetrical chute, and a more reliable system to bring the vehicle down safely. Below are the specifications of the main parachute chosen based on the parameters discussed above.

Table 14. Parachute parameters used to determine ideal sizing

	Air Density $[Slugs/ft^2]$	Dry Weight $[lbs]$	Terminal Velocity $[ft/s]$	Drag Coefficient	Surface Area $[ft^2]$
Main Parachute	.00189 (@1500 ft AGL)	90	22	2.2	167
Drogue Parachute	.00133 (@10,000 ft AGL)	90	90	0.6	17.5

Both the main and drogue parachutes interface with the recovery system through a single 3000 lb swivel between the shroud lines of the parachute and the shock cord. The lengths of the shock cord were selected to ensure that the rocket is stable during descent. A longer shock cord between the parachute and rocket yields a larger system moment of inertia, resulting in a more stable descent that is less susceptible to rocking or flipping. Sufficient length of shock cord is also needed during descent to ensure that the wake created by the rocket does not cause the parachute to collapse in on itself.

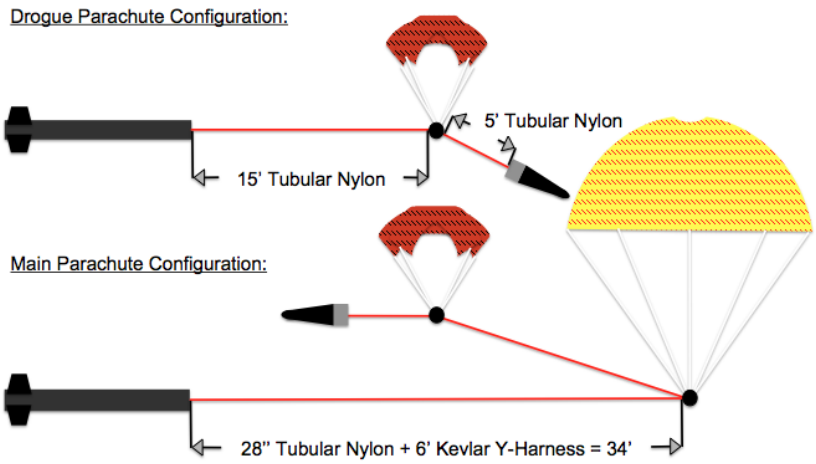

Figure 45. Shock Cord lengths for the recovery system depicted during the descent under the drogue and main parachute separately

The ejection system is used to eject the nosecone and recovery devices out of the recovery bay of the rocket by shearing the nylon pins holding the nosecone without causing damage to the recovery equipment.

High internal pressure is produced in the recovery compartment via means of rapid gas expansion in order to separate the nosecone, exposing the parachute to the airflow and deploying the chute. Small black powder ejection charges are reliable and used extensively by the industry to create this pressure. We will use pyrodex for its reliability in testing, cost, and availability, and are not concerned about inconsistent combustion since the charges will be detonated at a maximum altitude of 10,000 ft. The ejection pod is comprised of an aluminum bowl reinforced with Gorilla brand duct tape and ignition comes in the form of an e-match that is embedded in the pod.

The target pressure is determined by the free volume within the recovery compartment and the strength of the shear pins that will keep the nosecone attached to the rocket body. The strength of the shear pins is calculated using the modulus of elasticity of nylon and the cross-sectional area of the shear pin. From these parameters we use the ideal gas law to find the appropriate charge size in grams to effectively deploy the recovery system.

$$n = \frac{PV}{RT} \tag{14}$$

Table 15. Pyrodex P Ejection Charge Parameters

P	V	R	T
12 psi	3610 in^3	22.16 $\frac{ft-lb_f}{lbm-R}$	3307 R

The size of the ejection charge is calculated to be 4.5 grams assuming complete combustion of the pyrodex. The ejection pod (containing 7 grams of Pyrodex due to an added factor of safety determined empirically) is connected to binding posts that are mounted in the recovery bulkhead, allowing the ejection charge to be connected from the topside of the bulkhead without having to access the electronics bay.

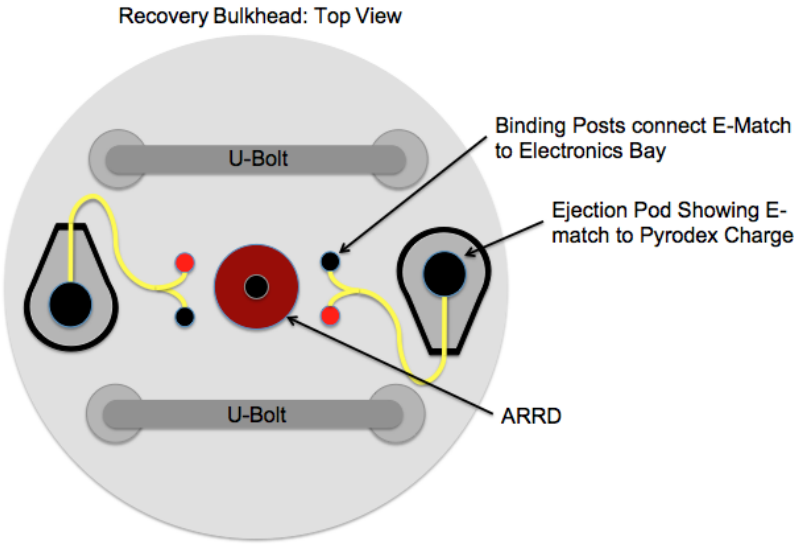

Figure 46. Ejection Pod Overview

2. Electronics Bay

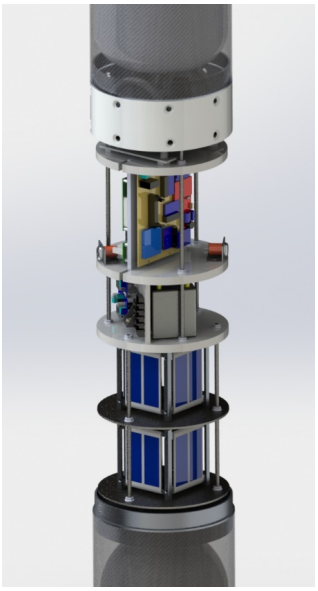

Figure 47. Electronics Bay

The section of our rocket that contains all of our flight computers, data acquisition and control computers is located underneath the upper recovery bay and is referred to as the electronics bay. The Electronics Bay or E-Bay contains the components responsible for firing the apogee and main parachute pyros, recording pressure transducer data from our hybrid engine, and safely igniting our hybrid engine with actuation of a servo.

The primary flight computer on Daedalus is a TeleMega purchased from Altus Metrum which in summary is "a high-end recording dual-deploy altimeter for high power model rocketry with integrated GPS".[7] While the GPS features will not be used for competition flight, the TeleMega will be operating the ignition of our ejection charge for the apogee parachute and the pyrotechnic separation of the ARRD system for the main parachute. Aside from recording altitude the TeleMega will also record acceleration data using an onboard sensor suite. The arming power switch for the TeleMega consists of a key-switch accessible from the exterior of the vehicle and is powered by an independent Lithium Polymer battery.

The secondary flight computer on Daedalus is the Stratologger CF produced by PerfectFlite which will be used as a redundant system ensuring firing of the apogee ejection charge and the ARRD system charge for the main parachute. The Stratologger CF will also be recording altitude during the flight allowing a comparison point for the TeleMega altitude estimate. The arming power switch for the Stratologger CF consists of a key-switch accessible from the exterior of the vehicle and is powered by an independent Duracell 9V battery.

The on-board control and DAQ computer board developed by our team consists of a "Control" Arduino Mini and a "DAQ" Arduino Mini which are responsible for safely actuating the servo of the hybrid engine and recording pressure transducer data during flight to on-board SD cards. The main "Control" Arduino is also responsible for serial communication to the remote launch system, which relay's information to our ground control station wirelessly. The main power switch for the On-Board Control & DAQ board is a key-switch accessible from the exterior of the vehicle and is powered by the 12.8 V Lithium Iron Phosphate (LiFePO) battery.

On Daedalus the hybrid engine Icarus uses the actuation of a servo motor in order to turn the ball

valve which initiates the flow of Nitrous Oxide through the combustion chamber. This ignites the engine and begins the combustion process of the Icarus hybrid engine. The power source for this servo is an independent 7.3 V Lithium Polymer contained in the Electronics Bay and has a key-switch for activating power along with a motor controller for disconnecting the battery circuit from the servo after actuation. The purpose behind our design utilizing a motor controller activated and deactivated by the on-board control computer is that Lithium Polymer batteries can be hazardous when fully discharged and in order to mitigate a risk of fire we use the motor controller to disconnect power to the servo after the servo has been actuated and fully opened. This action would mean that for the rest of the flight and recovery of the vehicle there would be no additional current draw from the Lithium Polymer battery and a low risk of a discharge fire.

Table 16. Electronics Power Requirements

Power Source	Device
12.8 V LiFePO	TeleMega Apogee Pyro
12.8 V LiFePO	TeleMega Main Pyro
3.7 V Li - Polymer	TeleMega Computer
9V Duracell	StratoLogger Apogee Pyro
9V Duracell	StratoLogger Main Pyro
9V Duracell	StratoLogger Computer
7.4 V Li - Polymer	Ball Valve Servo
12.8V LiFePO	Extinguishing Exp. Payload
12.8 V LiFePO	Pressure Transducer 1
12.8 V LiFePO	Pressure Transducer 2
5 V Reg. LiFePO	Arduino Mini "Control"
5 V Reg. LiFePO	Arduino Mini "DAQ"

3. GPS Module

In order to be able to track Daedalus during flight and after landing we will be utilizing the BeeLine GPS reciever developed by BigRedBee. This receiver operates on the 70cm amateur radio ham band and transmits APRS packets that are received by our ground tracking station which consists of a Baofeng UV-5R ham radio with a connection to a mobile application decoder called APRS-Droid. These packets allow the tracking station and eventually the chase team after landing to track the vehicle for recovery from the desert.

Due to the carbon fiber composition of the majority of our rocket and the fact carbon fiber is non-radio transparent, the nosecone was designed instead of fiberglass in order to allow the GPS Module to have radio transparency. What actually contains the BeeLine GPS inside of the vehicle's nosecone is a 100% density poly-jet 3D printed component which threads onto a female poly-jet 3D printed coupler that is epoxied into the fiberglass nosecone. This threaded piece allows the rocket tip and hence the GPS module to be removable in order to turn on the independent power supply of the BeeLine GPS before launch. The effectiveness of this design was flight tested during the October flight of Daedalus and our tracking station was able to receive APRS packets throughout flight and up to touch-down of the vehicle.

Figure 48. GPS Module

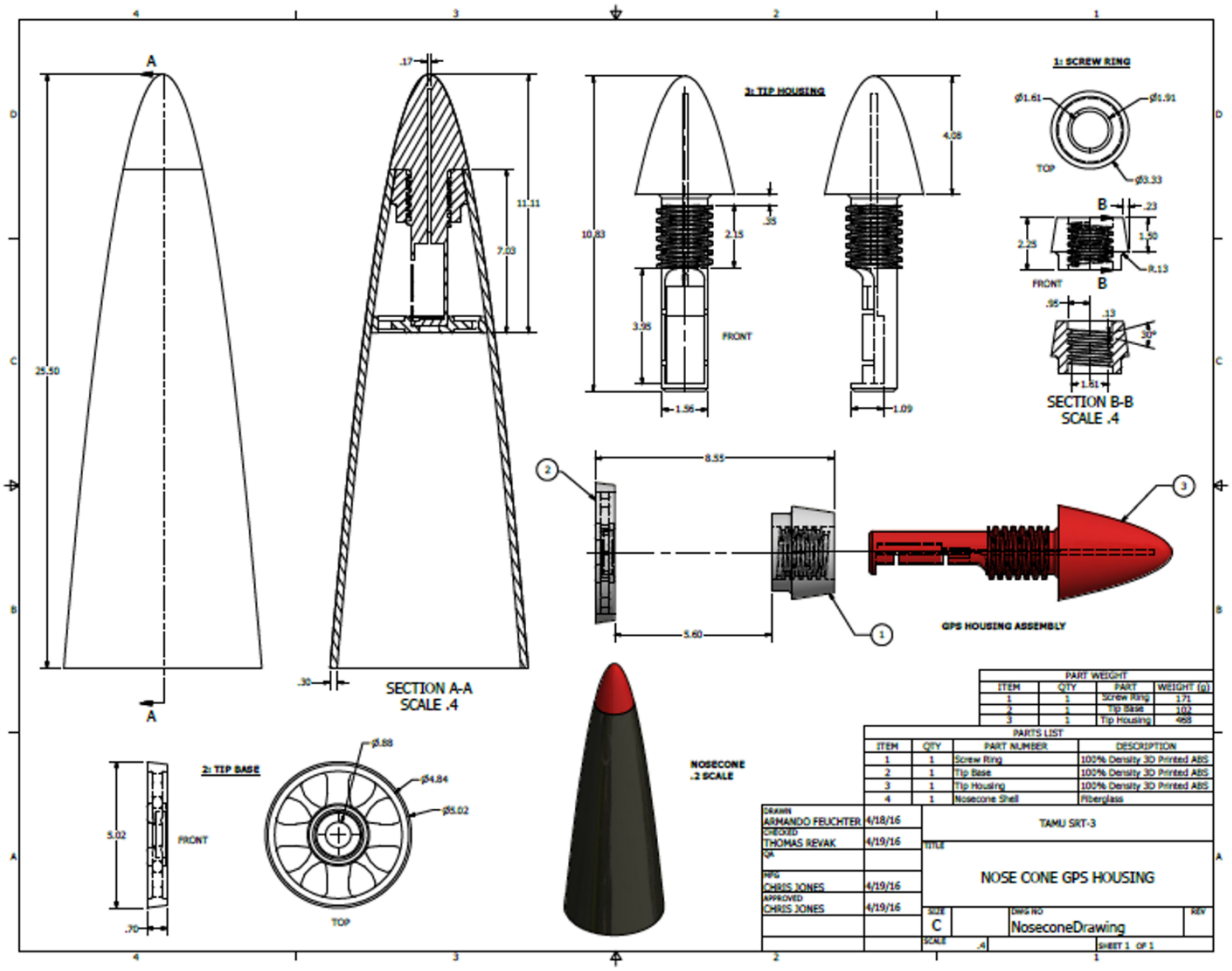

Figure 49. Drawing of GPS Module

D. Payload Subsystems

The payload bay is the portion of the vehicle that contains the experimental payloads we are flying for the current mission. A parameter that our payload bay was designed to meet is a standardized mounting geometry across all of our team's vehicles which would allow us to collaborate with other schools or groups in developing experimental payloads. The details of the mounting geometry along with all relevant information needed for developing a payload for our vehicle is detailed in the Interface Control Document (ICD) our team developed.

1. Experimental Payload - Bellair High School 9-DOF

Size Classification: U1 CubeSat or Smaller
Abstract: A payload intended for high-school students to gain experience in 3D-printing, programing, and developing a flight ready payload for data acquisition on a hybrid engine flight.
Details: Consists of an Arduino Feather, 3D printed components, Lithium Ion battery, and 9-DOF sensor.
Operations: The experiment provided by Bellair High School is powered on during final assembly of Daedalus and begins recording data from the 9-DOF sensor as soon as the Arduino is powered on. Following ICD requirements set by our team, the payload has enough battery and memory in the SD card in order to be functioning for several hours in case of any delays on the launch-pad.

2. Experimental Payload - Texas A&M SRT Extinguishing Experiment

Size Classification: U2 CubeSat or Smaller
Abstract: A payload intended to test the effects of a contained extinguishing agent under flight g-load in order to further develop payloads for vehicle automatic extinguishing methods.
Details: Consists of an Arduino Uno, 5V Servo, Raspberry PI 2, Raspberry PI Camera, Voltage Regulator, Pressurized 8 gram CO2 cartridge, extinguishing agent (sodium bi-carbonate NaHCO3/baking soda), plexiglass and steel frame.
Operations: The Extinguishing experiment is powered on along with main computers with an exterior key switch and after launch is triggered by the TeleMega auxiliary pyro channel which sends a signal down to the voltage regulator which is then read by the Arduino Uno's digital pin. Once the signal from the TeleMega is received the servo is actuated by the Arduino and releases pressure from the CO2 cartridge container and fills the enclosed and sealed plexiglass container with extinguishing sodium bi-carbonate. Throughout the flight a Raspberry PI camera will be filming the experiment in order to review the footage post-flight.

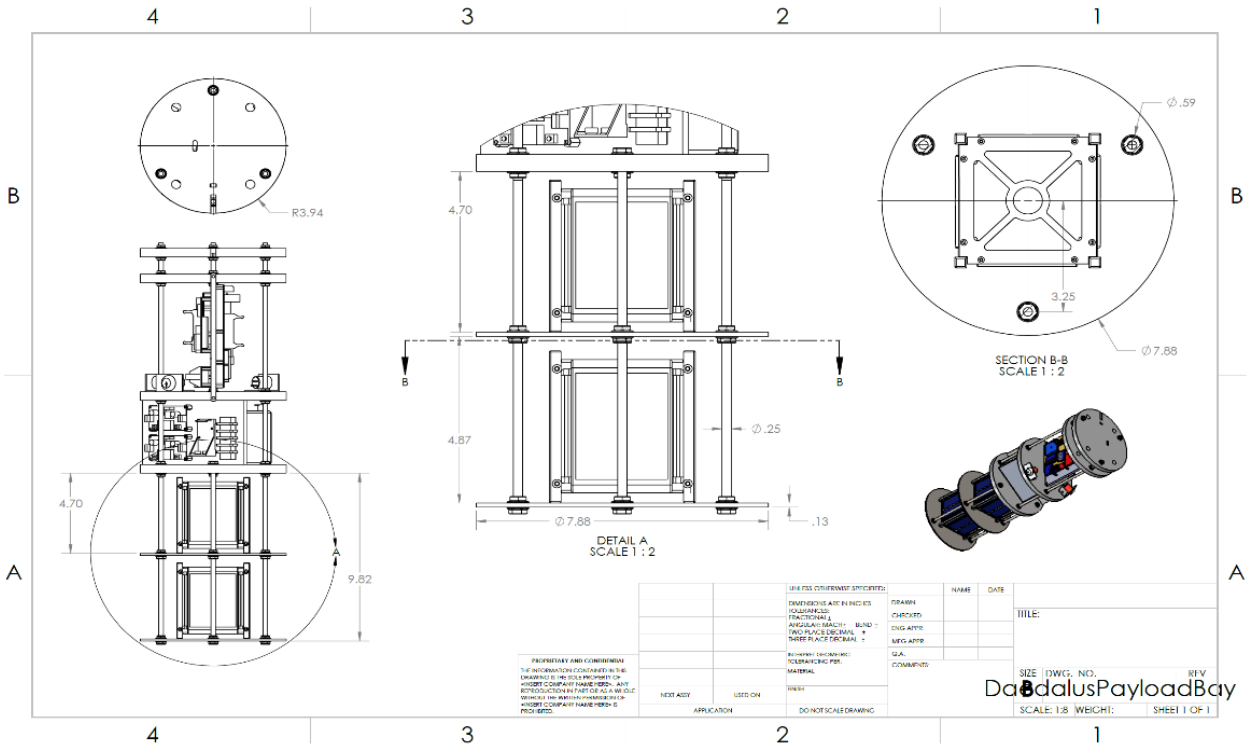

Figure 50. Daedalus Payload Bay

III. Mission Concept of Operations Overview

A. Description

There are four major subsystems that pertain to hybrid rocket launch operations. The Launch Control System (LCS) encompasses the custom built launch box, control and DAQ computers, and all RF communication infrastructure. The launch box is a system of relays and microprocessors that handle both command functions to the rocket and DAQ functions to and from the rocket and launch pad. The Oxidizer Loading System (OLS) is responsible for filling the flight tank and making sure the rocket is primed for lift off. OLS contains the oxidizer fill tank, the environmental control unit (hot box), fill and vent lines, and quick disconnects and its supporting pneumatic systems. The OLS is supported by the LCS for command relay purposes. The Flight Propulsion System (FPS) contains the oxidizer flight tank, plumbing, ball valve actuation unit, injector, combustion chamber, and supporting sensor package. The FPS is controlled through breakaway line connection with the LCS. The Propulsion Ignition System (PIS) provides the energetics to begin the combustion reaction of the FPS. PIS encompasses the ignitor and the oxygen priming unit. The Vehicle Recovery System (VRS) is defined as the primary and secondary COTS flight computers, GPS module, and all parachute, shock cords, release mechanisms, and ejection charges.

Figure 51 outlines the operational process of the remote launch system and the ground control station.

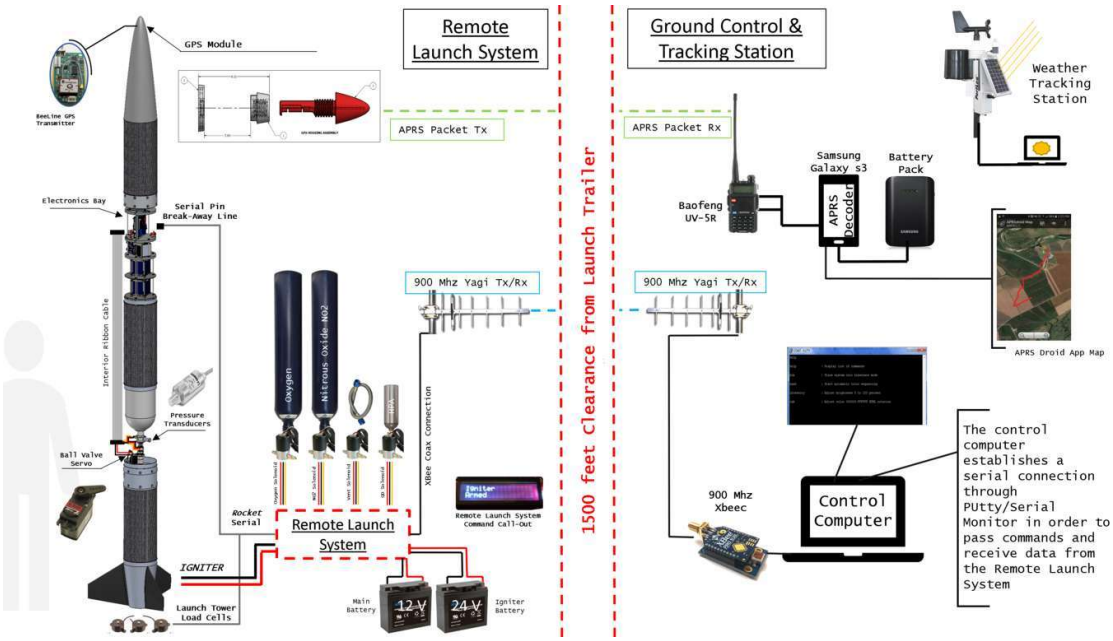

Figure 51. Overview of Electronic System Operations

Figure 52 graphically summarizes the mission phases.

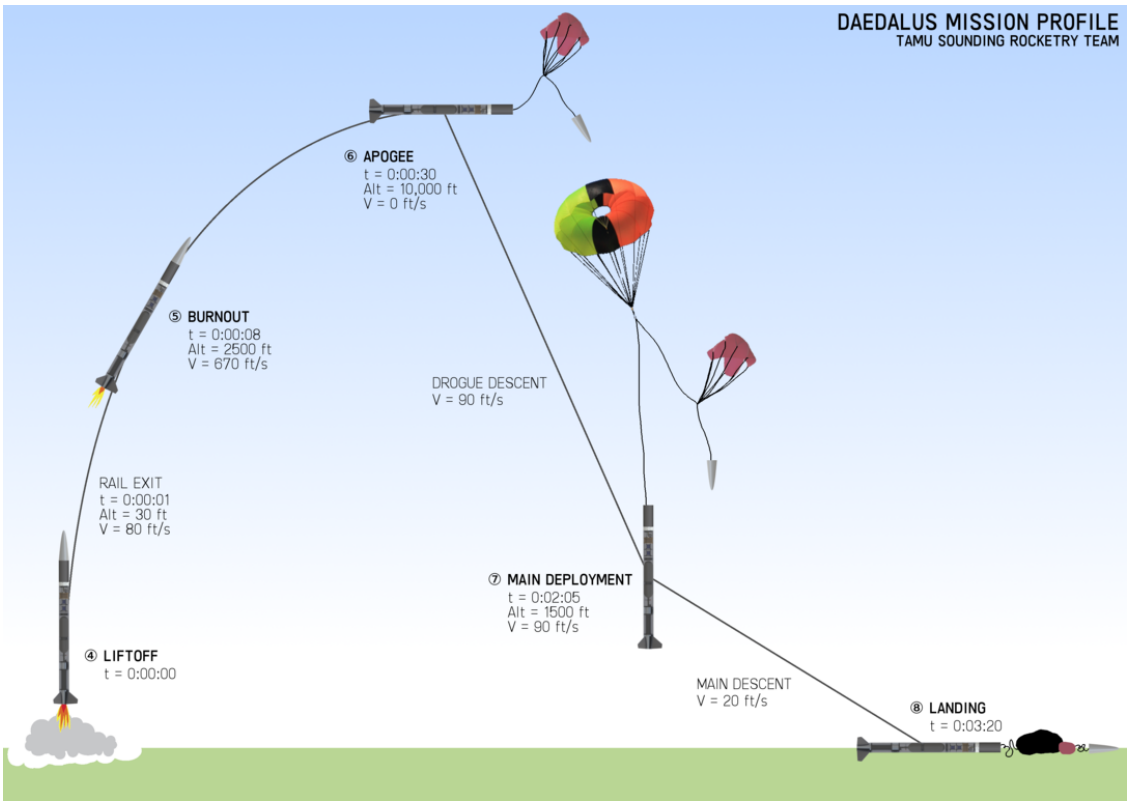

Figure 52. Daedalus Mission Profile, Phases 4-8

B. Definitions

Launch Control System - LCS - Launch box, computers
Oxidizer Loading System - OLS - Environmental control unit, fill tank, solenoids, QD
Flight Propulsion System - FPS - Oxidizer Tank, ball valve, combustion chamber
Propulsion Ignition System - PIS - Igniter, oxygen priming
Vehicle Recovery System - VRS - Flight computers, parachutes, GPS

Mechanical Safe - MS - Tank valves, tank regulators, turn keys/switches
Software Safe - SS - Digital command

C. Mission Phases

Assumptions: Rocket on pad, vertically installed
Energetic device safed and armed status are defined according to section 4 of the Spaceport America Cup *Intercollegiate Rocket Engineering Competition Design, Test, & Evaluation Guide*. Events listed in tables are the result of defining mission event.

1. *System Prime*

Defining mission event: Power provided to LCS/VRS

LCS	OLS	PIS	FPS	VRS
ARMED	SAFED	SAFED	NON-ENERGETIC	ARMED
Powered	2×MS, 2×SS	3×MS, 2×SS	Unpressurized	Powered
Check for RF Check igniter resistance	Fill Hose - *Connected* Vent Hose - *Connected* Oxidizer Fill Tank - *Closed* Solenoids - *Open*	Oxygen Tank - *Closed* Solenoids - *Closed* Igniter - *Installed/Shunted* Oxygen Sting - *Installed*	Ball Valve - *Closed* Oxidizer Tank - *Uncharged* Combustion Chamber - *Fuel loaded/greased*	Flight Computers - *Powered* Drogue Chute - *Internal* Main Chute - *Internal* Ejection Charges - *Installed*

personnel clear

2. *Fill*

Defining mission event: Command sent to open "N_2O Fill" solenoid

LCS	OLS	PIS	FPS	VRS
ARMED	ARMED	SAFED	SAFED	ARMED
Powered	Active	1×MS, 2×SS	1×MS, 2×SS	Powered
Recording load cell Recording engine pressures Maintain RF connectivity	Fill Hose - *Connected* Vent Hose - *Connected* Oxidizer Fill Tank - *Open* Solenoids - *Open*	Oxygen Tank - *Open* Solenoids - *Closed* Igniter - *Installed* Oxygen Sting - *Installed*	Ball Valve - *Closed* Oxidizer Tank - *Pressurized* Combustion Chamber - *Fuel loaded/greased*	Flight Computers - *Powered* Drogue Chute - *Internal* Main Chute - *Internal* Ejection Charges - *Installed*

3. Ignite

Defining mission event: Command sent to turn ball valve in rocket plumbing system which allows N_2O to flow into the combustion chamber from the internal oxidizer run tank

LCS	OLS	PIS	FPS	VRS
ARMED	SAFED	ARMED	ARMED	ARMED
Powered	1×MS, 2×SS	1×MS, 2×SS	Active	Powered
Maintain RF connectivity Record load cell Record engine pressures Send commands	Fill Hose - *Disconnected* Vent Hose - *Disconnected* Oxidizer Fill Tank - *Open* Solenoids - *Closed*	Oxygen Tank - *Open* Solenoids - *Open* Igniter - *Active* Oxygen Sting - *Active*	Ball Valve - *Open* Oxidizer Tank - *Pressurized* Combustion Chamber - *Ignited*	Flight Computers - *Powered* Drogue Chute - *Internal* Main Chute - *Internal* Ejection Charges - *Installed*

4. Liftoff

Defining mission event: Rocket clears launch tower and breakaway lines sever

LCS	OLS	PIS	FPS	VRS
ARMED	SAFED	SAFED	ARMED	ARMED
Powered	1×MS, 2×SS	1×MS, 2×SS	Active	Powered
Maintain RF connectivity Record load cell Record engine pressures Send commands	Fill Hose - *Disconnected* Vent Hose - *Disconnected* Oxidizer Fill Tank - *Open* Solenoids - *Closed*	Oxygen Tank - *Open* Solenoids - *Closed* Igniter - *non-energetic* Oxygen Sting - *non-energetic*	Ball Valve - *Open* Oxidizer Tank - *Pressurized* Combustion Chamber - *Pressurized*	Flight Computers - *Powered* Drogue Chute - *Internal* Main Chute - *Internal* Ejection Charges - *Installed*

5. Burnout

Defining mission event: Engine unchokes

LCS	OLS	PIS	FPS	VRS
SAFED	SAFED	SAFED	ARMED	ARMED
2×SS	1×MS, 2×SS	1×MS, 2×SS	Active	Powered
Maintain RF connectivity Send solenoid shutoff commands	Fill Hose - *Disconnected* Vent Hose - *Disconnected* Oxidizer Fill Tank - *Open* Solenoids - *Closed*	Oxygen Tank - *Open* Solenoids - *Closed* Igniter - *non-energetic* Oxygen Sting - *non-energetic*	Ball Valve - *Open* Oxidizer Tank - *Pressurized* Combustion Chamber - *Pressurized*	Flight Computers - *Powered* Drogue Chute - *Internal* Main Chute - *Internal* Ejection Charges - *Installed*

6. Apogee

Defining mission event: Command send to fire ejection charges

LCS	OLS	PIS	FPS	VRS
SAFED	SAFED	SAFED	NON-ENERGETIC	ARMED
2×SS	1×MS, 2×SS	1×MS, 2×SS	Active	Active
Maintain RF connectivity Send solenoid shutoff commands	Fill Hose - *Disconnected* Vent Hose - *Disconnected* Oxidizer Fill Tank - *Open* Solenoids - *Closed*	Oxygen Tank - *Open* Solenoids - *Closed* Igniter - *non-energetic* Oxygen Sting - *non-energetic*	Ball Valve - *Open* Oxidizer Tank - *Unpressurized* Combustion Chamber - *Unpressurized*	Flight Computers - *Powered* Drogue Chute - *Active* Main Chute - *Internal* Ejection Charges - *Activated*

7. Main Deployment

Defining mission event: Command send to fire Advance Retention Release Device charge

LCS	OLS	PIS	FPS	VRS
SAFED	SAFED	SAFED	NON-ENERGETIC	NON-ENERGETIC
2×SS	1×MS, 2×SS	1×MS, 2×SS	Active	Active
Maintain RF connectivity Send solenoid shutoff commands	Fill Hose - *Disconnected* Vent Hose - *Disconnected* Oxidizer Fill Tank - *Open* Solenoids - *Closed*	Oxygen Tank - *Open* Solenoids - *Closed* Igniter - *non-energetic* Oxygen Sting - *non-energetic*	Ball Valve - *Open* Oxidizer Tank - *Unpressurized* Combustion Chamber - *Unpressurized*	Flight Computers - *Powered* Drogue Chute - *Active* Main Chute - *Active* Ejection Charges - *non-energetic*

8. Landing

Defining mission event: Rocket body impacts ground

LCS	OLS	PIS	FPS	VRS
NON-ENERGETIC	SAFED	SAFED	NON-ENERGETIC	NON-ENERGETIC
Unpowered	2×MS	3×MS	Unpressurized	Pyros depleted
Maintain RF connectivity Send solenoid shutoff commands	Fill Hose - *Disconnected* Vent Hose - *Disconnected* Oxidizer Fill Tank - *Closed* Solenoids - *Closed*	Oxygen Tank - *Closed* Solenoids - *Closed* Igniter - *non-energetic* Oxygen Sting - *non-energetic*	Ball Valve - *Open* Oxidizer Tank - *Unpressurized* Combustion Chamber - *Unpressurized*	Flight Computers - *Powered* Drogue Chute - *Inactive* Main Chute - *Inactive* Ejection Charges - *non-energetic*

IV. Conclusions and Lessons Learned

Over the course of the year and the past four years of existence, the member of SRT have learned a great deal in terms of team management and technical skills. The team has also learned and begun implementing

ways to improve knowledge transfer to subsequent years.

A. Team Management Lessons Learned

For the management core, it is extremely important to understand the role of a manager is to implement tools to increase the efficiency of their members limited time. Learning the strengths and weakness of each team member as well as knowing their commitment capabilities and how they react to stress (go off the grid, complete items rapidly, do their best work, etc.), are critical to best assign tasks. Most members respond best to unified, one-track directions. Multi-pronged approaches are difficult to implement and require managers to be able to translate the multi-direction to typically "one-track minded" sub-teams.

Timelines at any level are difficult to maintain. It is critical for managers to understand all the timelines that feed into development of their timelines and to the overall team timeline. Availability of machines and machinists are difficult to know in advance and require careful planning by the machining party. Academic schedules are notorious for (rightly) getting in the way of team interests. It is also important to understand the timelines of supporting sub-teams for certain task or testing campaigns.

As the team grows, and more and more experience is built, it is important to develop effective, yet non-restricting version control methods for CAD and procedures. Additionally, maintaining and implementing quick recall posters or digital methods are important for efficient operations.

B. Technical Lessons Learned

A valuable lessoned learned from the the technical side of the team was the importance of cross-team communication. Many technical developments or modifications affect countless other individual task, so it is crucial that any change is made aware to the entire team so that relevant members can plan accordingly.

Another technical team lesson learned is the importance of members to take ownership of their work and have a mentality that they are the last point of contact with a given task. All tasks are important and doing the best possible work is critical to success of the entire team.

Testing components not only to specification defined by external parties (safety organizations, university, competition requirements), but in closest possible flight configuration is extremely valuable. Anything that can go wrong will go wrong, and if the kinks of these complex systems are not found in the configuration they will be used, they may never manifest themselves, and only be found in pieces across the desert floor. Also, if something has not failed before, does not mean it will fail now. This mentality promotes a rich safety environment.

C. Strategies for Knowledge Transfer

Accurate documentation is the most important thing a designing team can do for later years. With the loss of members a facet of university organizations, knowledge retention is key to the success and advancement of later years. Instructions and How-To guides provide steps to making sure future members can reproduce the work done be earlier years without time lost to determining working methods, order of operations, or configuration. For testing, standardizing test reports for easily accessible information eliminates time guessing about the specifics of critical tests. A flexible platform that aids in taking detailed, potentially graphical notes is a Microsoft office program called OneNote. This has become and will continue to evolve into a comprehensive knowledge base for readily accessible data.

Younger member recruitment is another method of investment for knowledge retention. By educating younger members, the team spends the extra time to explain basic principles older members learn in later classes, but the younger members carry the information with them to explain to later years when the time comes. Consequently, member retention is key to the success of the team. Time investments made must pay off by members staying on the team and bringing the information with them. This ensures the ideas and time of the current members are respected and that they are rewarded with technical knowledge and personal skills they will use in their future careers.

Acknowledgments

The accomplishments of the Sounding Rocketry Team are due in part to the continued support and guidance of Dr. Adonios Karpetis (Department of Aerospace Engineering, Texas A&M University), Dr. Rodney Bowersox (Department of Aerospace Engineering, Texas A&M University), Dr. Thomas Pollock (Department of Aerospace Engineering, Texas A&M University).

References

[1]Knacke, T.W.. Parachute Recovey Systems Design Manual. Naval Weapons Center, China Lake, 1992. Print.

[2]Sadeck, J., and Lee, C., 'Continuous Disreefing Method for Parachute Opening', Journal of Aircraft, vol. 46, 2009, pp. 1-4.

[3]Parachutes, H., 'How to make a Parachute — Fruity Chutes!', Fruitychutes.com. ¡https://www.fruitychutes.com/help_for_parachutes/how_to_make_a_parachute.htm.¿

[4]Nakka, R., 'Richard Nakka's Experimental Rocketry Site', Nakka-rocketry.net http://www.nakka-rocketry.net/paracon.html.

[5]Machine, Monterey. "RATTworks: Precision Hybrid & Tribrid Rocket Motors - Accessories." RATTworks: Precision Hybrid & Tribrid Rocket Motors - Accessories. Monterey Machine Products, 2006. Web. 19 Feb. 2017.

[6]Foster, Thomas. "Tubular Nylon Webbing 1"." Strapworks.com. Volusion, n.d. Web. 19 Feb. 2017.

[7]https://altusmetrum.org/TeleMega/

[8]Stoney,William., Transonic Drag Measurements of eight body-nose shapes, NACA RM l53K17, 5 February 1954

[9]Toft, Hans. "Nose Cone Drag Study for the SStS Rocket." (2005): 10. Sugar Shot to Space Program Documentation. Sugar Shot to Space. Web. 10 Oct. 2014. ¡http://sugarshot.org/downloads/nosecone_drag_study_ss2s_rocket.pdf¿.

[10]Owens, Robert. "Aerodynamic Characteristics of Spherically Blunted Cones at Mach Numbers from 0.5 to 5.0." NASA Technical Note D-3088 (1965). Print.

[11]Suliman, M. A., O. K. Mahmoud, M. A. Al-Sanabawy, and O. E. Abdel-Hamid. "Computational Investigation of Base Drag Reduction for a Projectile at Different Flight Regimes."ASAT-13-FM-05 (n.d.): n. pag. Military Technical College, Kobry Elkobbah, Cairo, Egypt, 2009. Web. ¡http://www.mtc.edu.eg/ASAT13/pdf/FM05.pdf¿.¿

[12]Hennin, Bart. "Why Should You Airfoil Your Rocket's Fins?" Peak of Flight Newsletter 305 (2012): n. pag. Apogee Rockets, 31 Jan. 2012. Web. 28 Oct. 2015.

[13]Harris, Charles D., NASA Supercritical Airfoils: A Matrix of Family-Related Airfoils, NASA Technical Paper 2969, Hampton, Virginia, January 1990.

[14]"Launching Safely in the 21st Century." National Association of Rocketry. 29 Oct. 2009. Web. 27 Oct. 2015.

[15]Fernandez, M. M., Propellant Tank Pressurization Modeling for a Hybrid Rocket, Thesis, Mechanical Engineering Dept., Rochester Institute of Technology, Rochester, NY, 2009.

[16]Newlends, R., Modelling the nitrous run tank emptying, Aspire Space

[17]Doran, E., Dyer, J., Lohner, K., Dunn, Z., Cantwell, B., Nitrous Oxide Hybrid Rocket Motor Fuel Regression Rate Characterization, 42nd AIAA/ASME/SAE/ASEE Joint Propulsion Conference, AIAA, Sacramento, CA, July 2006.

[18]Bellomo, Barato, Faenza, Lazzarin, Bettella, and Pavarin, Numerical and Experimental Investigation on Vortex Injection in Hybrid Rocket Motors, AIAA 2011-5675, 2011.

[19]Sutton, G. P., Biblarz, O., Rocket Propulsion Elements, 9th ed. , Wiley, Hoboken, New Jersey, 2017, pp. 156-161, 593-619.